Recalibration and Assessment of the SNPP CrIS Instrument: A Successful History of Restoration after Midwave Infrared Band Anomaly

Flavio Iturbide-Sanchez, *Senior Member, IEEE*, Larrabee Strow, David Tobin, Yong Chen, Denis Tremblay, Robert O. Knuteson, David Johnson, Clayton Buttles, Lawrence Suwinski, Bruce P. Thomas, Adhemar Rivera, Erin Lynch, Kun Zhang, *Member, IEEE*, Zhipeng Wang, Warren Porter, Xin Jin, Joe Predina, *Life Member, IEEE*, Reima Eresmaa, Andrew Collard, Benjamin Ruston, James A. Jung, Christopher D. Barnet, Peter Beierle, Banghua Yan, Daniel Mooney and Henry Revercomb

***Abstract*— The Suomi National Polar-orbiting Partnership (SNPP) Cross-track Infrared Sounder (CrIS) has provided critical observations for environmental applications for nearly 10 years. However, on 26 March 2019, the Joint Polar Satellite System (JPSS) Interface Data Processing Segment (IDPS) stopped producing the operational SNPP CrIS Sensor Data Record (SDR) product due to a failure of the midwave infrared (MWIR) band. Following a comprehensive risk assessment, the switch from primary to redundant Side-2 electronics was made on 24 June 2019, successfully recovering the full capabilities of the sensor. Comprehensive assessment results demonstrate the high quality of the CrIS SDR product resulting from the sensor recalibration, thus meeting the JPSS Level-1 requirements with margin. The spectral calibration prioritized consistency with the CrIS SDR product prior to the side switch in order to minimize the impact on users. Results show that the radiometric impact in the CrIS SDR product resulting from the side switch is not significant and is within the calibration radiometric uncertainty. It is demonstrated that after the instrument restoration, the SNPP CrIS SDR product recovers the quality needed to be used as radiometric reference for the calibration and validation of infrared remote sensing instruments. The recovery of the SNPP CrIS MWIR band is expected to support improvements in numerical weather forecasting by restoring the MWIR band channels sensitive to tropospheric water vapor. This should also help to maintain continuity and redundancy of one of the backbone observations of the global observing system.**

The scientific results and conclusions, as well as any views or opinions expressed herein, are those of the author(s) and do not necessarily reflect those of NOAA or the Department of Commerce. This work was supported by the Joint Polar Satellite System Program Office. *(Corresponding author: Flavio Iturbide-Sanchez.)*

Flavio Iturbide-Sanchez, Yong Chen, and Banghua Yan are with the NOAA/NESDIS/Center for Satellite Applications and Research, College Park, MD 20740 USA (e-mail: flavio.iturbide@noaa.gov; yong.chen@noaa.gov; banghua.yan@noaa.gov).

Larrabee Strow is with the University of Maryland at Baltimore County, Baltimore, MD 21250 USA (e-mail: strow@umbc.edu).

David Tobin, Robert O. Knuteson, James A. Jung and Henry Revercomb are with the University of Wisconsin at Madison, Madison, WI 53706 USA (e-mail: dave.tobin@ssec.wisc.edu; robert.knuteson@ssec.wisc.edu; jim.jung@noaa.gov; hankr@ssec.wisc.edu).

Denis Tremblay, Erin Lynch, and Kun Zhang are with the Global Science and Technology, Inc., Greenbelt, MD 20770 USA (e-mail: denis.tremblay@noaa.gov; erin.lynch@noaa.gov; kun.zhang@noaa.gov).

David Johnson is with the NASA Langley Research Center, Hampton, VA 23681 USA (e-mail: David.G.Johnson@nasa.gov).

Clayton Buttles, and Lawrence Suwinski are with the L3Harris Technologies, Inc., Fort Wayne, IN 46818 USA (e-mail: Clayton.Buttles@l3harris.com; Lawrence.Suwinski@l3harris.com).

Bruce P. Thomas is with the NOAA/NESDIS/Office of Satellite and Product Operations, Suitland, MD 20746 USA (e-mail: bruce.p.thomas@noaa.gov).

Adhemar R. Rivera is with the NOAA/NESDIS/Joint Polar Satellite System Program Office, Lanham, MS 20706 USA (e-mail: adhemar.rivera@noaa.gov).

Zhipeng Wang, and Peter Beierle are with University of Maryland at College Park, Earth System Science Interdisciplinary Research Center (ESSIC), 5825 University Research Ct, College Park, MD 20740 USA (e-mail: zhipeng.wang@noaa.gov; peter.beierle@noaa.gov).

Warren Porter, and Xin Jin are with the Science Systems and Applications, Inc., Lanham, MD 20706 USA (e-mail: warren.porter@noaa.gov; xin.jin@noaa.gov).

Joe Predina is with the Logistikos Engineering LLC 623, Fort Wayne, IN 46845 USA (email: joe.predina@logistikosengineering.com).

Reima Eresmaa is with the Finnish Meteorological Institute, FI-00101 Helsinki Finland (e-mail: Reima.Eresmaa@fmi.fi).

Andrew Collard is with the I. M. Systems Group, Rockville, MD 20852 USA (e-mail: andrew.collard@noaa.gov).

Benjamin Ruston is with the U.S. Naval Research Laboratory, Washington, DC 20375 USA (e-mail: Ben.Ruston@nrlmry.navy.mil).

Christopher D. Barnet is with the Science and Technology Corp., Columbia, MD 21046 USA (e-mail: chrisdbarnet@gmail.com).

Daniel Mooney is with the Massachusetts Institute of Technology Lincoln Laboratory, Lexington, MA 02421-6426 USA (e-mail: mooney@ll.mit.edu).

Index Terms— **Cross track Infrared Sounder, Joint Polar Satellite System, Suomi National Polar-Orbiting Partnership, Infrared Observations, Calibration, Remote Sensing, Satellite, Numerical Weather Forecasting.**

I. Introduction

THE CrIS sensor on-board the National Oceanic and Atmospheric Administration (NOAA)/Joint Polar Satellite (JPSS) series satellites is a Fourier transform spectrometer based on a 0.8 cm^{-1} optical path difference (OPD) Michelson interferometer. Currently, two CrIS sensors are in operation, one on the S-NPP satellite launched in October 2011 and the other on the NOAA-20 satellite launched in November 2017.

Both satellites fly on nearly sun-synchronous polar orbits at an ascending node equator crossing time of 13:30 PM locally with a separation phase of 180 degrees. The CrIS sensor has three spectral bands: the long-wave infrared (LWIR) band (650-1095 cm^{-1}), the mid-wave infrared (MWIR) band (1210-1750 cm^{-1}), and the short-wave infrared (SWIR) band (2155-2550 cm^{-1}). For each band, CrIS measures the infrared (IR) spectra from the Earth scene (ES) with a 3×3 detector array, corresponding to 9 field-of-views (FOVs) with 14-km diameter at nadir or one field-of-regard (FOR). With a scan mirror rotating in cross-track direction, the CrIS full Earth view scan angle is ±48.33°, resulting in a CrIS swath width on Earth of approximately 2,200 km. For each scan, CrIS collects 30 ES FORs, two FORs of deep space (DS) observations (cold radiometric reference) and two FORs of a warm blackbody radiometric reference, called internal calibration target (ICT) [1]. When operated in full-spectral resolution (FSR) mode, the measured interferograms are recorded with the same OPD. Under this mode, the CrIS SDR spectra are processed to have an unapodized Sinc spectral response function. The spectra are then Nyquist sampled with spectral sampling (distance between adjacent samples) and corresponding spectral resolution of 0.625 cm^{-1} (Rayleigh criterion) for all three bands. This results in a total of 2211 channels [2].

A. Identification of the MWIR Band Anomaly.

On 23 March 2019, the first instance of missing SNPP CrIS MWIR interferograms in the raw data record (RDR) associated with the MWIR band anomaly was detected. Invalid SNPP CrIS MWIR SDR data was observed in 1 scan on March 23, in 4 scans on March 24, and in 33 scans on 25 March 2019. Root cause analysis identified a potential point of failure in the MWIR band signal processor (SP) field programmable gate array (FPGA) and associated circuitry. These circuitries located in the Side-1 electronics reported intermittent single event functional interrupt (SEFI) and wake-up errors that eventually lead to the MWIR SP circuit card assembly (CCA) being held in reset on 26 March 2019. On the same day, the Interface Data Processing Segment (IDPS) stopped producing the SNPP CrIS SDR product due to a reduction in the amount of data available for IDPS SDR processing. Nine days prior to the first signs of the SNPP CrIS MWIR band failure, an anomaly was observed on the SNPP Advanced Technology Microwave Sounder (ATMS) scan drive (SD) main/compensator motor that resulted in large peaks in the electric current and power consumption. However, the anomaly investigation found little evidence to suggest that the SNPP ATMS anomaly was the root source. Additionally, little correlation between major space weather activity and the occurrence of the midwave anomaly on March 23rd was found. The most probable root source of the MWIR SP CCA circuit was associated with a single-event hard error. In an attempt to resolve the issue, power cycles were performed first on the MWIR band SP and then the entire CrIS instrument. However, this did not solve the problem.

B. Performing the Switch to Side-2 Electronics.

While production of operational LWIR) and SWIR SNPP CrIS SDR data resumed on 16 April 2019, the MWIR SDR data remained unavailable. To rectify the instrument anomaly and restore the full capabilities of the SNPP CrIS instrument, a formal decision to switch from the Side-1 to the Side-2 electronics was made on 21 June 2019 after assessing the potential impacts of performing the side switch during the hurricane season. On 24 June 2019, the switch to Side-2 electronics was initiated. At around 18:50 UTC, the instrument was transitioned from nominal mode to operational mode producing full spectral resolution (FSR) data for all the three

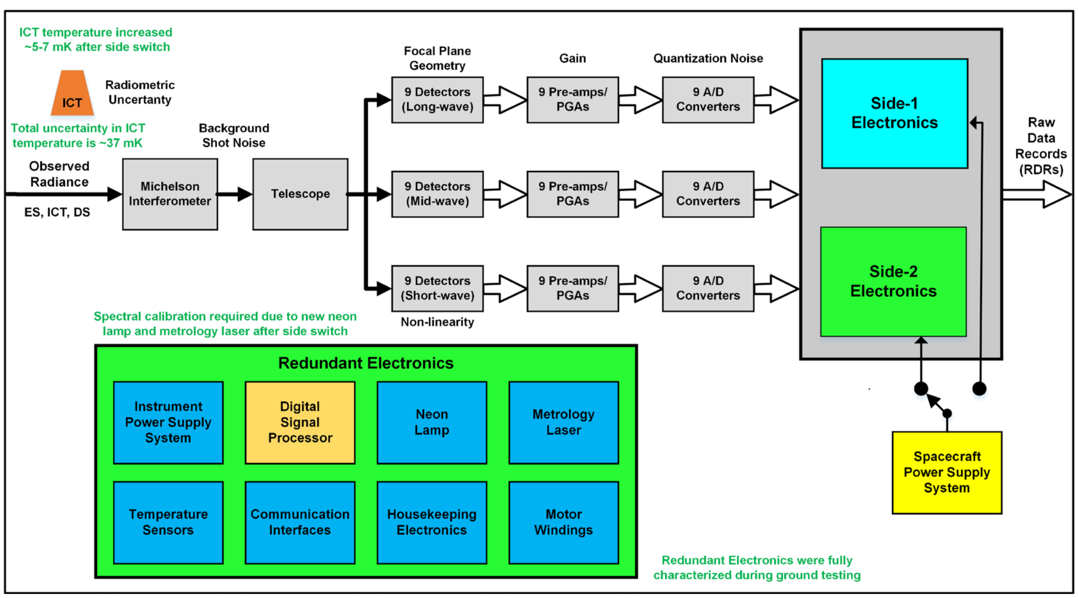

Fig. 1. Schematic of the main subsystems, modules and components of the CrIS sensor, illustrating its operation under the Side-2 electronics configuration.

instrument spectral bands. On 26 June 2019, the SDR products were suitable for preliminary science quality check and the SNPP CrIS SDR data product became available in the Government Resource for Algorithm Verification, Independent Test, and Evaluation (GRAVITE) system.

Fig. 1 shows a schematic representation of the main subsystems, modules and components of the CrIS sensor, illustrating its operation under the Side-2 electronics configuration. The main components of the redundant electronics are identified. This includes the digital signal processor (root source of the MWIR band failure when the sensor was operating under Side-1 configuration), as well as the neon lamp and metrology laser, critical for the instrument spectral performance. Switching to the redundant electronics introduces new temperature sensors used to estimate the thermodynamic temperature of the ICT for the instrument radiometric calibration.

Following the completion of Side-2 active commanding on 28 June 2019, the science quality check started. The CrIS SDR calibration and validation team began an intensive period of review and monitoring to quickly restore the SNPP CrIS SDR product to operational quality. Evaluation of the first two weeks of SNPP CrIS SDR Side-2 product, following the switch to Side-2 electronics, demonstrated that it held the JPSS beta level quality.

The SNPP CrIS SDR Side-2 data product was declared provisional with the upload of engineering packet (EP) version 40 (v40) on 1 August 2019 at 16:49:40 UTC. This engineering packet provided corrected mapping angles that brought the geolocation of CrIS observations within specification and updated spectral calibration parameters to match the Side-1 performance for the continuity of the mission data. Spectral calibration was required due to new Side-2 metrology laser, neon lamp and slight changes in the instrument temperature associated with different power consumption of redundant electronics. Low impact to the radiometric calibration was observed due to minor changes in the on-board ICT temperature, while no changes to the detector's nonlinearity coefficients were required.

The successful restoration of the sensor capabilities relied heavily on the Side-2 calibration constants derived during ground testing. The availability of quality calibration parameters was a key factor in the prompt recalibration of the sensor. *Fig. 2* shows the timeline of major events toward

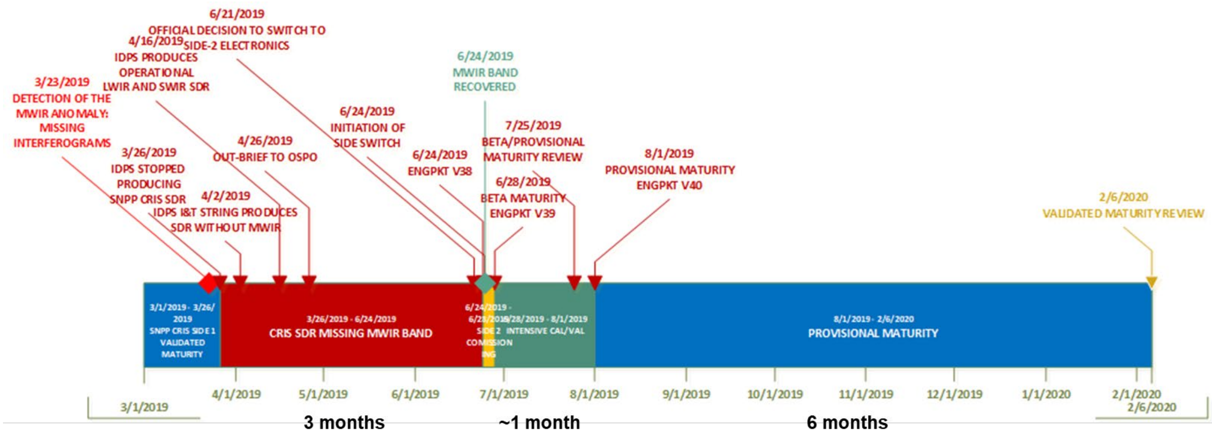

Fig. 2. Timeline of major events during the restoration of the SNPP CrIS instrument, indicating the loss of the MWIR band, the recalibration and initial validation activities along with a 6 months period to dedicated to demonstrate the long-term stability of the sensor and the calibrated observations.

the restoration of the SNPP CrIS instrument, which includes nearly 3 months of missing MWIR observations, approximately 1 month of recalibration and initial validation activities after the MWIR band recovery and 6 months of validation activities to demonstrate the long-term stability of the calibrated observations. These activities were concluded on 6 February 2020, when the SNPP CrIS SDR Side-2 product reached the JPSS Validated Maturity level after demonstrating the long-term stability of the SNPP CrIS sensor and the long-term radiometric, spectral and geolocation quality of the SDR data product, based on validation findings and user feedback. This paper reviews the restoration and recalibration of the SNPP CrIS sensor as well as the long-term assessment of the SDR product after the sensor side switch.

The organization of the manuscript correspond to the order in which the instrument restoration, recalibration and assessment of the SNPP CrIS SDR product was performed. Section II presents details of the SNPP CrIS sensor spectral calibration and its assessment. Section III and IV report the evaluation of the radiometric and noise performance, respectively, following the instrument side switch. An overview of the geolocation calibration and the evaluation of the geolocation uncertainty is presented in Section V. Section VI provides a discussion about the impact and benefits of restoring the full capabilities of the SNPP CrIS sensor, while the main conclusions of this work are described in Section VII.

II. Spectral Calibration and Assessment

During the side switch period, a significant effort was taken in adjusting the Side-2 spectral calibration parameters in order to maintain the same effective spectral calibration of the radiances before and after the side switch. The spectral calibration process attempts to reduce both the relative spectral shifts among FOVs and the absolute spectral errors due to its impact on the radiometric quality of the SDR data. Reducing the spectral errors improves the FOV-to-FOV radiometric consistency as well as the radiometric bias, critical for data usage in NWP models. The main calibration changes needed after the switch to Side-2 electronics were the adjustment of the neon wavelength and small changes to the focal plane alignment relative to the interferometer optical axis. Both of these affect the spectral calibration. The Side-2 electronics use a different neon calibration lamp. Thermal vacuum (TVAC) testing more than a decade ago showed that the Side-2 lamp had a slightly different alignment relative to the interferometer optical axis, and possibly a slightly different geometric emission profile. The differential effective alignment of the Side-2 versus the Side-1 neon lamp introduced a relative spectral offset of ~4.15 ppm, measured during SNPP TVAC testing. However, as will be explained later, the neon calibration of SNPP on Side-1 had shifted by about 0.4 ppm from mission start. Initial testing after the switch to Side-2 indicated that the on-orbit neon calibration was within 0.1 ppm of the Side-2 TVAC value. Therefore, in order to match calibration before and after the Side switch, the Side-2 neon lamp wavelength was adjusted (reduced) by 0.4 ppm. In addition, since the focal plane alignment changed due to the Side switch, the in-track, cross-track, and a small radially symmetric shift of the focal plane positions were also applied in order to bring the spectral scale of all off-axis FOVs to the FOV-5 effective on-axis calibration. SNPP was switched to the Side-2 electronics on 24 June 2019 at which point spectral recalibration could commence. In order to minimize impacts of the Side-2 electronics on users, a decision was made to choose spectral calibration coefficients (which include the neon wavelength and detector positions relative to the interferometer optical axis) that minimized changes to the radiances relative to the Side-1 spectral calibration. This decision did not provide the best absolute spectral calibration, since the SNPP Side-1 neon had drifted about 0.4 ppm since the beginning of the mission. Moreover, detector radially symmetric offsets relative to the interferometer optical axis produced equivalent offsets in radiance space with a maximum of slightly more than 1 ppm. These differences are extremely small and have little to no impact on users. But, for maximum consistency, the spectral calibration was set as close as possible to the Side-1 values.

The FOV5 (center FOV within the focal plane array) spectral calibration is essentially independent of any in-track/cross-track errors in the focal plane position, and therefore these detectors are only sensitive to neon calibration offsets. Due to that, FOV5 spectral shifts are used to determine the adjustment of the effective neon wavelength. After changing the neon lamp calibration to the TVAC Side-2 value, all three bands were re-calibrated. The spectral calibration is performed by comparing clear ocean-only upwelling spectra to spectra computed using the Stand-alone AIRS Radiative Transfer Algorithm (SARTA) [3] and atmospheric profiles based on ECMWF forecast/analysis model fields. This approach is detailed in [4], which cross-correlates those observed and computed radiances and finds the shift in the computed radiance spectrum that produces the highest cross-correlation. That shift, in ppm units, is used to determine the neon bulb effective wavelength and the radial positions of each FOV for each band relative to the interferometer optical axis. The SNPP CrIS observed ppm offsets for the 3 bands times 9 detectors/band were measured for the day of 3 March 2019 (before the Side-1 midwave electronics failure) and for 29 June 2019 after the Side-2 electronics had been made operational. Changes to the neon lamp and focal plane positions were derived by fitting the differences in the detector offsets, in ppm, between March 3 and June 29, in order to achieve high stability and continuity in the SNPP CrIS SDR data product, as discussed above.

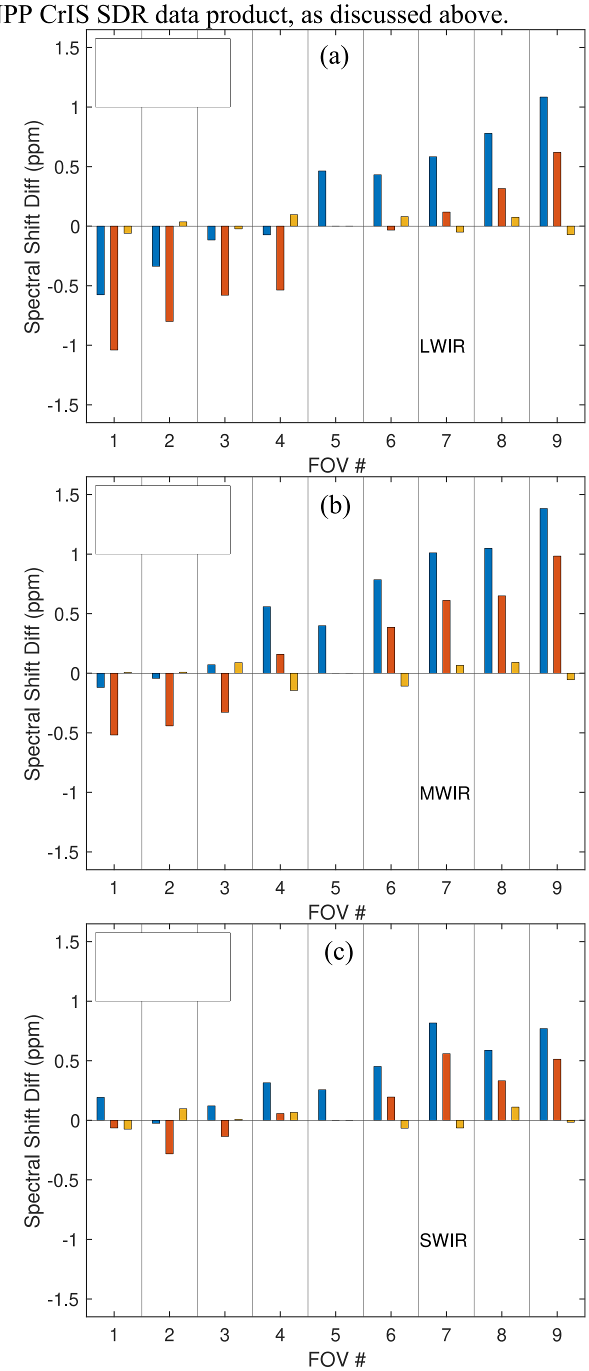

Fig. 3. Spectral shifts, in ppm, associated with each SNPP CrIS detector after switch to Side-2 electronics, and after adjusting the neon lamp frequency by 4.15 ppm (as indicated by TVAC results) for the (a) LWIR, (b) MWIR, and (c) SWIR bands for all SNPP CrIS 9 FOVs. The blue bars correspond to observed shifts, the red bars are the detector spectral shifts minus the FOV5 spectral shift value, and yellow bars illustrate the spectral shifts (observed minus calculated) after fitting for in-track and cross-track translations of each focal plane and a simultaneous radial scaling of each FOV. The final neon value was adjusted by the residual of ~0.4 ppm, observed in the absolute shift of the FOV5, in order to bring agreement with the Side-1 neon wavelength.

Fig. 3 shows the observed ppm differences for all detectors, separated by the LWIR, MWIR and SWIR focal planes. Blue bars show the measured differences. The FOV5 offsets are almost the same for all three focal planes with a magnitude of about 0.4 ppm. For this test, the neon wavelength had already been switched to the Side-2 value from TVAC results. Therefore, these small spectral offsets, observed in the three spectral bands, demonstrate the accurate pre-launch characterization of the sensor and the minimal impact suffered by the instrument from the pre-launch activities to the deployment of the sensor on-orbit. The final neon wavelength used after validation of the Side-2 switch was modified to remove this 0.4 ppm difference in order to achieve consistency with the Side-1 neon wavelength. The red bars in *Fig. 3* have the FOV5 neon related offset removed in order to illustrate the ppm offsets to the observed radiances caused by a shift in the focal plane/detector positions due to the Side-2 switch. Of course, we do not expect the relative geometry of the focal plane to change, so these changes are due to in-track and cross-track shifts in the focal plane position, and possibly due to a slight change in the telescope focus (radial term). A very clear pattern with FOV ID number is seen in these plots with high similarity between focal planes (larger spectral shifts for corner FOV1 and FOV9 with opposite sign). This pattern is indicative of an in-track shift in the focal plane.

TABLE *1*
CHANGES (SIDE-2 MINUS SIDE-1) IN FOCAL PLANE POSITIONS (CROSS-TRACK ANDIN-TRACK) AND RADIAL SCALING (TELESCOPE FOCUS)

Band	*Cross-track, dx (μrad)*	*In-track, dy (μrad)*	*Radial, dr (μrad)*
LWIR	12.7 ± 3.9	30.2 ± 4.0	10.0 ± 2.8
MWIR	6.8 ± 5.0	30.7 ± 5.0	-7.9 ± 3.6
SWIR	0.2 ± 4.3	16.4 ± 4.3	-6.7 ± 3.0

These values correspond to the changes in the alignment of the SNPP CrIS detectors relative to the interferometer focal plane optical axis, observed after the instrument side switch. All units are in microradians (μrad). The uncertainties in the focal plane movements are given as 2-σ estimates.

A non-linear regression [4] was used to minimize these ppm offsets for each focal plane (LWIR, MWIR and SWIR), with three free parameters: (a) in-track shift, (b) cross-track shift, and (c) a radial-only shift in the FOV positions, which attempts to mimic any slight changes in the telescope focus. Therefore, we have three free parameters fitting eight observations (all FOVs except FOV5). The yellow bars in *Fig. 3* correspond to the residuals after these fits. Clearly, these three parameters are sufficient to largely remove any ppm offsets. TABLE *1* lists the fitted parameters and their 2-σ uncertainties. The in-track movements are the largest and are far larger than the statistical uncertainties of the fit. These shifts are relatively similar between focal planes, especially between the LWIR and MWIR. The radial shifts are the average radial shift (meaning a radial shift in the in-track and cross-track plane) for the corner and side FOVs. The radial shifts appear to be statistically significant. If the radial shifts are not included in the fits, the observed and calculated spectral differences (yellow bars) of the mean ppm offsets increase by a factor of 20. If the radial offsets are included the mean ppm offsets over FOVs (mean of fit residual results in *Fig. 3*) are reduced to the 0.01 ppm level, far below the absolute accuracy of the observed ppm errors. Although we have set the frequency calibration parameters for Side-2 to produce nearly identical results to Side-1 operation, this does not mean that the Side-2 frequency calibration will stay identical, since small long-term drifts in the neon and in the focal plane positions are possible. These observed shifts between Side-1 and Side-2 frequencies due to the alignment of the detectors relative to the interferometer focal plane optical axis are presumably associated with the slightly different thermal environment caused by the different power consumption between the Side-1 and Side-2 electronics modules.

The long-term evaluation of the spectral performance of the instrument 9 FOVs is reported in *Fig. 4* using an independent spectral calibration algorithm that is used to derive the spectral calibration, but following the same general methodology [5]. This figure presents the absolute spectral shift during 2019 for the three instrument spectral bands. A spectral shift reduction among the 9 FOVs as well as spectral consistency between Side-1 and Side-2 is achieved for the three spectral bands after the upload of the optimized Side-2 spectral calibration coefficients contained in the EP version 40. For the LWIR and SWIR bands, the long-term peak-to-peak spectral shift among the 9 FOVs is within 1.5 ppm, and within 2.5 ppm for the MWIR band. Those results clearly satisfy with sufficient margin the spectral quality requirement for the CrIS SDR data, which is 10 ppm for each band. TABLE 2 provides the spectral performance in the form of the bias and standard deviation of the absolute spectral shift associated with each FOV and band during 2019. The maximum difference in the systematic component (bias) of the spectral offset between Side-1 (before the MWIR band anomaly) and Side-2 (after the upload of EP version 40), for a particular FOV, is not greater than 0.8, 0.5 and 0.25 ppm for the LWIR, MWIR and SWIR bands, respectively. The random variability of the spectral offset for each detector is also within 0.2 ppm for Side-1 and Side-2. These results demonstrate the high spectral stability achieved between the Side-1 and Side-2, after an effective spectral calibration optimized for maximum spectral consistency.

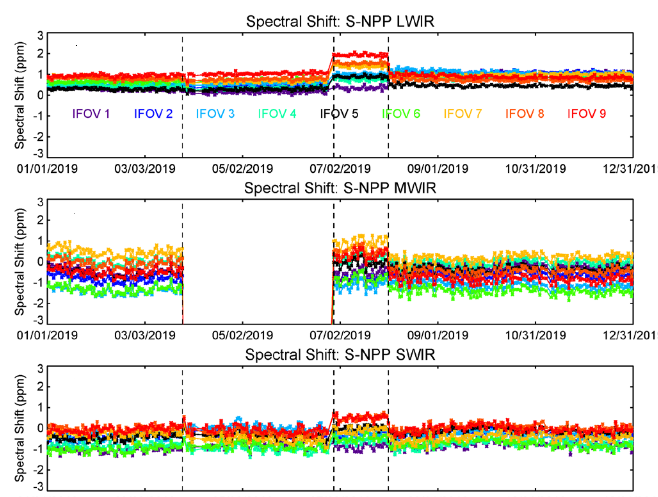

Fig. 4. Daily absolute spectral shift for the (a) LWIR, (b) MWIR, and (c) SWIR bands for all SNPP CrIS 9 instantaneous Fieldof-Views (IFOVs) during 2019. The vertical lines indicate the loss of the Side-1 MWIR band (26 March 2019), the upload of the EP version 39 (28 June 2019) and the upload of the EP version 40 (1 August 2019), respectively.

TABLE 2
LONG-TERM ABSOLUTE SPECTRAL SHIFT BIAS AND STANDARD DEVIATION, IN PPM, OF THE SNPP CRIS SDR DATA, GIVEN FOR EACH INSTRUMENT BAND AND FOV, DURING 2019.

Band/FOV	Side-1 (EPv37) (ppm)	Side-1 MWIR Failure (ppm)	Side-2 (EPv39) (ppm)	Side-2 (EPv40) (ppm)	Bias difference: Side-2 (EPv40) minus Side-1 (EPv37) (ppm)
LW/FOV1	0.3 ± 0.07	0.15 ± 0.06	0.35 ± 0.08	1.04 ± 0.08	0.74
LW/FOV2	0.43 ± 0.06	0.41 ± 0.06	0.8 ± 0.06	1.1 ± 0.07	0.67
LW/FOV3	0.48 ± 0.06	0.57 ± 0.07	1.02 ± 0.05	1.1 ± 0.09	0.62
LW/FOV4	0.47 ± 0.07	0.33 ± 0.06	0.74 ± 0.06	0.8 ± 0.07	0.33
LW/FOV5	0.29 ± 0.05	0.28 ± 0.06	0.9 ± 0.05	0.46 ± 0.06	0.17
LW/FOV6	0.64 ± 0.05	0.73 ± 0.07	1.45 ± 0.05	0.9 ± 0.09	0.26
LW/FOV7	0.82 ± 0.07	0.68 ± 0.07	1.39 ± 0.06	0.97 ± 0.07	0.15
LW/FOV8	0.8 ± 0.06	0.76 ± 0.06	1.54 ± 0.05	0.73 ± 0.07	-0.07
LW/FOV9	0.94 ± 0.06	1.03 ± 0.07	1.93 ± 0.06	0.9 ± 0.09	-0.04
MW/FOV1	-0.43 ± 0.19	N/A	-0.56 ± 0.22	-0.24 ± 0.17	0.19
MW/FOV2	-0.82 ± 0.19	N/A	-0.79 ± 0.2	-0.64 ± 0.17	0.18
MW/FOV3	-1.38 ± 0.18	N/A	-1.13 ± 0.21	-1.14 ± 0.17	0.24
MW/FOV4	0.04 ± 0.19	N/A	0.18 ± 0.2	-0.05 ± 0.17	-0.09
MW/FOV5	-0.5 ± 0.19	N/A	-0.05 ± 0.19	-0.38 ± 0.17	0.12
MW/FOV6	-1.32 ± 0.19	N/A	-0.81 ± 0.2	-1.41 ± 0.17	-0.09
MW/FOV7	0.48 ± 0.2	N/A	0.95 ± 0.22	0.19 ± 0.18	-0.29
MW/FOV8	-0.05 ± 0.2	N/A	0.5 ± 0.2	-0.48 ± 0.17	-0.43
MW/FOV9	-0.51 ± 0.19	N/A	0.32 ± 0.21	-0.84 ± 0.18	-0.33
SW/FOV1	-1.02 ± 0.15	-0.85 ± 0.17	-0.86 ± 0.16	-0.82 ± 0.17	0.2
SW/FOV2	-0.39 ± 0.14	-0.17 ± 0.18	-0.26 ± 0.13	-0.27 ± 0.16	0.12
SW/FOV3	-0.42 ± 0.17	0.02 ± 0.19	-0.23 ± 0.16	-0.33 ± 0.17	0.09
SW/FOV4	-0.85 ± 0.14	-0.99 ± 0.17	-0.61 ± 0.12	-0.77 ± 0.17	0.08
SW/FOV5	-0.45 ± 0.13	-0.35 ± 0.16	0.04 ± 0.12	-0.13 ± 0.15	0.32
SW/FOV6	-1.01 ± 0.15	-0.85 ± 0.17	-0.47 ± 0.13	-0.76 ± 0.17	0.25
SW/FOV7	-0.22 ± 0.16	-0.53 ± 0.18	-0.08 ± 0.14	-0.45 ± 0.18	-0.23
SW/FOV8	-0.01 ± 0.15	-0.2 ± 0.18	0.52 ± 0.12	0.04 ± 0.17	0.05
SW/FOV9	-0.06 ± 0.15	-0.06 ± 0.19	0.51 ± 0.13	-0.04 ± 0.18	0.02

III. RADIOMETRIC CALIBRATION ASSESSMENT

For the SNPP CrIS instrument, the primary radiometric uncertainty (RU) contributors are the calibration blackbody temperature, the calibration blackbody reflected radiance terms, and the detector nonlinearity [6]. After the instrument side switch, the main radiometric impact to the CrIS RU was associated with the change from using Side-1 ICT Platinum Resistance Thermometers (PRTs) to using a different set of ICT PRT sensors from Side-2. Other than the ICT PRTs, the other components of the calibration chain (e.g. the blackbody itself, detectors and detector electronics chain) are physically the same for Side-1 and Side-2 operations. Another factor is the instrument temperature which may be affected during the period of operation before the switch to Side-2, where the Side-1 MWIR band processing electronics was not operating, and other subtle changes in instrument temperature from Side-1 to Side-2 operations. However, unlike other sensor designs, the majority of the CrIS sensor operates at uncontrolled ambient temperature and experiences a range of temperatures on a regular basis, and so small changes in operating temperature do not have a significant impact on the calibration uncertainty. This section reports the evaluation of the radiometric impact after the instrument side switch via the comprehensive analysis of the FOV-to-FOV radiometric changes and analysis of the long-term radiometric performance. Comparisons against simulated CrIS radiances and observations from other infrared sensors, including MetOp-B Infrared Atmospheric Sounding Interferometer (IASI), Aqua Atmospheric Infrared Sounder (AIRS) and the SNPP Visible Infrared Imaging Radiometer Suite (VIIRS) instruments, are presented and discussed here.

A. *FOV-to-FOV Radiometric Consistency*

FOV-to-FOV analyses encompass various studies to assess the calibration of one of the nine FOVs of CrIS against the others. The major purpose of performing the FOV-to-FOV analysis is to assess the radiometric consistency between the FOVs after the instrument side switch. All Side-2 results reported in this section are based on operational EP version 40.

The performed FOV-to-FOV radiometric analysis consisted in comparing Side-1 spectra collected from March 22 to March 23 of 2019 (before the MWIR band anomaly) and Side-2 spectra collected from June 29 to July 1 of 2019 (after the instrument side switch). All CrIS FOR that meet the following conditions are included: latitude range 60S-60N, 13<=FOR#<=18 (near nadir), and the standard deviation over the 3x3 of FOVs at 900 cm^{-1} is less than 3 $mW/(m^2\ str\ cm^{-1})$. For this analysis, the relative FOV-to-FOV radiometric difference was computed by subtracting the center FOV (FOV5) from each of the nine FOVs on every 3x3 FOR. The mean of a large statistical set is used to reduce the fluctuations caused by cloud spatial variability. The mean difference of each FOV from the center FOV is compared before and after the SNPP side switch. This result is presented in *Fig. 5* as the Side-1 minus Side-2 relative FOV difference shown as the mean and standard deviation over the nine detectors in each spectral band. This result of this analysis indicates there is no statistically significant change in the FOV-to-FOV radiometric consistency between SNPP Side-1 and Side-2.

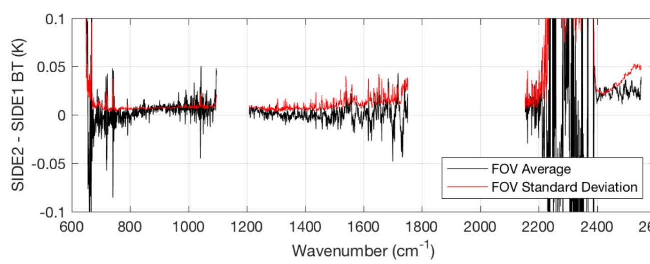

Fig. 5. The change in the relative FOV-to-FOV radiometric reproducibility between Side-1 and Side-2 using the center FOV (FOV5) as the reference.

In order to assess the long-term FOV-to-FOV radiometric consistency, the daily mean brightness temperature has been computed for each FOV. This result is used to derive the daily radiometric consistency relative to FOV5, as presented in *Fig. 6*. In this case, three representative FOVs, FOV2 (a side FOV), FOV7 (a corner FOV) and FOV5 (center FOV), as well as three frequencies representative of each CrIS spectral band (900 cm^{-1}, 1210 cm^{-1}, and 2182 cm^{-1}) have been selected. The selection of FOV7 is based on the fact that this is the most nonlinear detector over the MWIR band while FOV2 is highly linear. In this respect, the small radiometric change over the side-switch would be a strong indicator that the nonlinearity remains unchanged. Note that the detectors and preamplifiers do not change with the CrIS switch therefore the nonlinear characteristics are not expected to change. *Fig. 6* clearly shows the long-term stability and consistent radiometric performance of FOV2 and FOV7 before the MWIR anomaly and after the side switch. These results also show that the FOV-to-FOV consistency of FOV2 and FOV7 relative to FOV5 is less than ±0.05K, over the three selected frequencies. For the SWIR FOV7, a slight radiometric increase, relative to FOV5, is observed just after the side switch. This radiometric change is not significant (~0.025K) and reduced around October 2019.

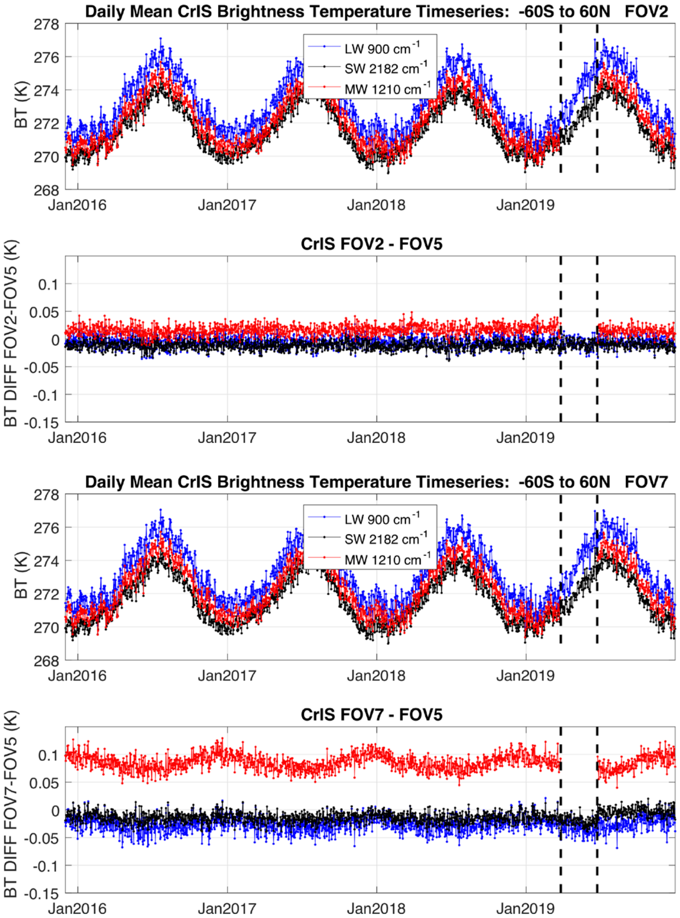

Fig. 6. The daily mean brightness temperature for FOV2, and FOV7 for the 900 cm^{-1}, 1210 cm^{-1}, and 2182 cm^{-1} frequencies, observed from the 60 degrees south latitude to 60 degrees north latitude. Also plotted is the radiometric difference of FOV2 and FOV5 with respect to the daily mean brightness temperature of FOV5. As a reference, the vertical dash lines indicate the period of the MWIR band loss from March 26 to June 24 of 2019. The long-term performance cover from December 2015 to January 2020.

Another long-term radiometric analysis was carried out by deriving the daily mean brightness temperature for two representative spectral ranges within each CrIS spectral band from January to December 2019. In this case, the analysis has the purpose of observing the long-term stability and performance of all FOVs over spectral regions that span the three CrIS spectral bands. These regions include two CO_2 absorption regions over the LWIR and SWIR bands (672-682 cm^{-1} and 2350-2370 cm^{-1}), two atmospheric window regions over the LWIR and SWIR bands (830-840 cm^{-1} and 2500-2520 cm^{-1}), and two water vapor absorption regions over the MWIR band (1382-1408 cm^{-1} and 1585-1600 cm^{-1}). The result is shown in *Fig. 7* in the form of the FOV-to-FOV radiometric difference, relative to FOV5. Just as it is shown in *Fig. 6*, this result confirms a FOV-to-FOV consistency within 0.05 K between Side-1 and Side-2, over the selected CrIS spectral regions. Over the 672-682 cm^{-1} LWIR band, where the impact of instrument nonlinearity changes could be clearly observed, radiometric changes smaller than 0.02K are identified between both sides. This includes the slight increase in the radiometric differences for FOV7. For the MWIR band, a data gap is observed due to the MWIR band anomaly. However, these results show the radiometric consistency achieved just after the successful recovery of the MWIR band (indicated by the second vertical dashed) with a FOV-to-FOV variability within ±0.05 K before and after the instrument side switch. The SWIR results help to identify reduced long-term FOV-to-FOV radiometric variability in the 2350-2370 cm^{-1} spectral region after the instrument side switch, mainly due to changes in the FOVs 1, 6, 7, 8. This could be associated with the radiometric impact of the Side-2 spectral calibration, which included a new neon lamp calibration system.

Fig. 7. Long-term radiometric trending of the FOV-to-FOV for Side-1 and Side-2 for selected regions across the SNPP CrIS spectral bands from January to December 2019. The first vertical dashed line indicates the time of the actual loss of the MWIR band on 26 March 2020, while the instrument was operating under Side-1 electronics. The second vertical dashed line corresponds to the day when the MWIR band was recovered on 24 June 2019, after the side switch. The third vertical dashed line indicates the actual day when the latest calibration parameters were uploaded on 1 August 2019, as part of EP v40.

TABLE *3*
SUMMARY OF THE OVERALL PERFORMANCE OF THE SNPP CRIS SIDE-1 AND SIDE-2 DATA AT FULL SPECTRAL RESOLUTION. THE REQUIREMENTS ARE REPORTED IN PARENTHESIS ALONG WITH THE DATA PERFORMANCE.

Band	Spectral Range (cm^{-1})	Spectra Resolution (cm^{-1})	Number of Channels	NEdN(1) Side1/Side2 (mW/m^2/sr/cm^{-1})	Spectral Uncertainty Side1/Side2 (ppm)	Geolocation Uncertainty(2) Side1/Side2 (km)	Radiometric Uncertainty(3) @287K BB(4) Side1/Side2 (%)	Radiometric Stability @287K BB(4) Side1/Side2 (%)
LWIR	650-1095	0.625	713	0.101/0.099 (0.14)	1.5/1.5 (10)	0.6/0.6 (5)	0.16/0.16 (0.45)	0.17/0.17 (0.40)
MWIR	1210-1750	0.625	865	0.0522/0.0536 (0.084)	2.5/2.5 (10)	0.6/0.6 (5)	0.19/0.19 (0.58)	0.21/0.21 (0.50)
SWIR	2155-2550	0.625	633	0.00741/0.00752 (0.014)	1.5/1.5 (10)	0.6/0.6 (5)	0.40/0.40 (0.77)	0.28/0.28 (0.64)

(1) Mean value averaged over 9 FOVs and over entire band.
(2) Geolocation uncertainty is based on the largest 3-sigma value found over all scan angles (FORs). Accounts for in-track and cross-track errors.
(3) SNPP radiometric uncertainty (RU) does not account for the polarization correction effect. RU values with polarization correction are expected to be lower than those reported in the table.
(4) The radiometric uncertainty and stability are relative to the radiance from a 287 K blackbody (BB) target.

The results derived from the FOV-to-FOV radiometric analysis demonstrate the instrument non-linearity consistency between Side-1 and Side-2, as well as the long-term radiometric stability achieved after the side switch. All observed radiometric changes are well within the estimated SNPP CrIS instrument radiometric uncertainty of 0.16, 0.19K, and 0.40K for the LWIR, MWIR and SWIR band, respectively (Table *3*) [7]. These radiometric results were important to determine that no further optimization of the non-linearity was required after the SNPP CrIS side switch.

B. SNPP CrIS/VIIRS Radiometric Comparisons

SNPP CrIS and VIIRS radiometric comparisons were used to characterize the CrIS calibration change due to the use of the new Side-2 ICT PRTs. Comparisons between SNPP CrIS and VIIRS observations are generated routinely. Daily match files are created after proper spectral and spatial transformation are applied so that both sensors observe the same scene over the same spectral response functions at VIIRS bands I05 (11.45 µm), M13 (4.05 µm), M15 (10.763 µm) and M16 (12.013 µm). Spatially uniform scenes are selected, with a very large number of collocated comparisons available each day. Using SNPP CrIS/VIIRS data from 5 days prior to and 5 days after the side switch on 24 June 2020, the double difference between CrIS Side-2 and CrIS Side-1 (CrIS Side-1 minus VIIRS from 5 days of comparisons prior to side switch minus CrIS Side-2 minus VIIRS from 5 days of comparisons after the side switch) as a function of scene brightness temperature, for a range of scene temperatures between 200 K and 320 K, was assessed and is presented in *Fig. 8*. The mean radiometric differences in the CrIS calibration from Side-1 to Side-2 are within ±10 mK for most scene temperatures but not generally statistically significant from zero. This demonstrates not only the Side-1 vs Side-2 radiometric consistency, but also show the positive impact of the effective pre-launch characterization and calibration of the Side-2 PRTs. At scene temperatures close to 280 K, however, which is close to the nominal ICT temperature, consistent and statistically significant radiometric changes between 5 to 7 mK are observed for all bands presented in *Fig. 8*.

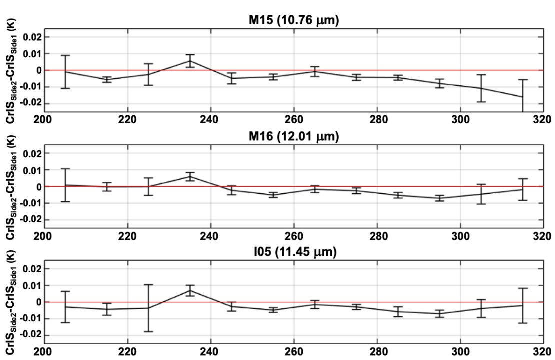

Fig. 8. Mean radiometric difference between SNPP CrIS Side-2 and CrIS Side-1 as a function of scene brightness temperature derived from comparisons between CrIS and VIIRS observations at band M15 (10.76 µm), M16 (12.01 µm), and I05 (11.45 µm). For Side-1, 5 days prior to the side switch (June 19-23, 2019) were used. For Side-2, 5 days after the side switch (June 25-29, 2019) were employed. The error bars represent two standard deviations (K=2) within the selected binned scene temperatures.

Based on the historical data record of SNPP CrIS/VIIRS comparisons, this radiometric performance was not observed previously, when the SNPP CrIS instrument was operating under Side-1 electronics. This particular result suggests changes in the measured ICT temperature, most likely due to the change of ICT PRTs after the instrument side switch. Quantitatively, those radiometric changes are well within the 1-sigma estimated total uncertainty of the ICT measured temperature (37 mK), where the PRTs uncertainty contribution is about 19 mK [6]. This is a remarkable result, that shows how well the CrIS design and instrument redundancy has worked in this respect and demonstrates that the radiometric calibration uncertainty for Side-2 is nearly the same for Side-1.

C. Radiometric Comparisons between Observations and Simulations

The radiometric impact of the instrument side switch is investigated using the double difference method and considering radiative transfer simulations as the radiometric transfer reference. This type of radiometric comparisons has the advantage of performing the impact study over the entire global domain and is not limited to a particular region. Simulated SNPP CrIS radiances at full spectral resolution were generated using the Community Radiative Transfer Model (CRTM) model and geophysical products from the European Center for Medium-range Weather Forecasts (ECMWF) 3-h analysis/forecast global model data with 91 levels and 0.25 x 0.25 degree spatial resolution. The difference between observed and CRTM simulated radiances were calculated at the collocated CrIS FOVs. The double difference is an indirect comparison method that requires a stable transfer reference [8]. In order to achieve this condition, the radiometric comparisons were limited to homogeneous clear scenes, over ocean, within ±65°latitude. This strategy contributes to reduce the radiometric errors associated with the modeling of cloud fields, surface temperature, as well as surface emissions and reflections from land, ice and snow surfaces. Homogenous clear scenes were obtained using a hyperspectral infrared cloud detection algorithm based on [9] which has been successfully applied to CrIS observations as described in [5]. The algorithm has the capability to effectively identify cloud-contaminated scenes taking advantage of the pre-calculated observation-minus-simulation IR radiance differences. The cloud detection scheme does not rely on visible spectral information. In order to remove the effect of solar radiation on the simulated radiance, only clear-sky CrIS FOVs over ocean surface at nighttime were selected. The radiometric difference between SNPP Side-1 and Side-2 can be estimated using the double difference method, as expressed in Equation (1),

$$DD_{NPP,i} = \langle BT_{18,side1} - BT_{18,B} \rangle_i - \langle BT_{19,side2} - BT_{19,B} \rangle_i \quad (1)$$

where $BT_{18,side1}$ and $BT_{18,B}$ represent the daily SNPP observed and simulated spectra, respectively, in brightness temperature in year 2018, when the instrument was operating under Side-1 electronics. Similarly, $BT_{19,side2}$ and $BT_{19,B}$ represent SNPP observed and simulated spectra, for the same day when $BT_{18,side1}$ and $BT_{18,B}$ where obtained, but during 2019 and when SNPP was functioning using the instrument Side-2 electronics. The symbol $\langle \quad \rangle_i$ is used to represent the daily average operation. If the daily averaged simulations for 2018 and 2019 were statistically equivalent, the radiometric bias (systematic error) associated with the simulations would be cancelled out in the double difference process, thus providing the actual mean radiometric difference, at all channels, due to instrument side switch. However, due to the intrinsic radiative transfer model errors and biases in the input atmospheric profiles, particularly in the trace gases, the double difference in Equation (1) includes the residual simulation bias combined with the radiometric impact due to the SNPP side switch. In order to minimize the effect of the residual simulation bias, the effective radiometric difference for the SNPP side switch is estimated as

$$\delta_i = DD_{NPP,i} - DD_{N20,i} \tag{2}$$

where $D_{N20,i}$ is the double difference calculation similar to Equation (1) but using the NOAA-20 CrIS observations and the collocated CRTM simulations during the same comparison period. This idea is verified here using daily global data collected over several months. The double difference for the NOAA-20 CrIS ($D_{N20,i}$) serves as a reference for measuring the radiometric performance of the SNPP side switch, because the NOAA-20 CrIS has almost identical hardware design as the SNPP Side-1/Side-2 and operates in almost the same orbit as SNPP, with the half-orbit along-track separation. Furthermore, the NOAA-20 CrIS SDR data holds similar quality to SNPP CrIS SDR data and reached the validated maturity level on 14 August 2018. Since the same version of CRTM model was used in the simulation and the ECMWF 3-h analysis/forecast global model remained the same in 2018 and 2019, the model simulation biases have nearly the same effect in the calculations of $D_{NPP,i}$ and $D_{N20,i}$. Due to that, the effect of the CRTM model error and the simulation input biases is minimized when comparing the double difference calculations for the SNPP and the NOAA-20, as defined in Equation (2). Thus, the effective radiometric difference δ_i should mainly reflect the radiometric differences between the SNPP and NOAA-20 CrIS SDR data and the errors introduced into the statistics of the δ_i estimate, primarily associated with random processes. The possible sources of random errors include 1) the instrument noise levels of SNPP and NOAA-20, 2) the varying degrees of daily global coverage by the SNPP and NOAA-20 observations, and 3) undetected cloud contamination of the SNPP and NOAA-20 observations. These random errors can be reduced by averaging the sample δ_i estimates over all days when the double differences are calculated. The overall mean effective radiometric difference for all channels can be obtained by calculating the sample mean ($\bar{\delta}$). The uncertainty can be assessed by the standard deviation (σ) of the δ_i samples. In this study, the sample standard deviation (σ) is used to measure the amount of variability for *N* samples of δ_i deviated from the sample mean ($\bar{\delta}$).

The observed and simulated radiances were computed on a daily basis for the August 15 to December 31 timeframe, for the years 2018 (Side-1) and 2019 (Side-2), respectively. During the 2019 August-December period, the SNPP CrIS instrument was operating under Side-2 electronics, since the side switch was fully completed at the end of June 2019. The number of daily selected data points is ~90,000 and ~12 million in total between mid-August and the end of December. This dataset is statistically sufficient for this study. During this period, there is a total of *N*=139 samples (or days) ($i = 1,2,..,N$) available for determining the effective radiometric impact statistics. Here, the sample mean ($\bar{\delta}$) is used to represent the long-term effective radiometric impact of the SNPP side switch. For comparison purposes, the effective radiometric difference was determined using two contiguous periods, where the SNPP instrument was operating under Side-1 electronics. In this case, the 2018 September-October and November-December periods were selected to determine the Side-1 effective radiometric difference. This radiometric difference was defined as $\bar{\delta_1}$. *Fig. 9* shows the long-term effective radiometric difference due to the SNPP side switch ($\bar{\delta}$) along with the Side-1 effective radiometric difference ($\bar{\delta_1}$). The reported standard deviation characterizes the uncertainty of $\bar{\delta}$. It is evident that the side switch radiometric impact is quite small at the LWIR and MWIR bands (< 0.02 K) and within the statistical uncertainty of the selected approach. It is possible that some of the radiometric impact reported in *Fig. 9* comes from the effect of assimilating CrIS observation into ECMWF. However, this effect is expected to be minimal due to (1) the bias correction applied to the CrIS observations before the assimilation process, (2) the contributions from other assimilated observations, (3) the fact that no CrIS SWIR channels and only a few CrIS channels over the MWIR band are assimilated by ECMWF (less than 40 channels, as described in Section VI) and (4) the small radiometric impact associated with the side switch, verified in this manuscript using other approaches. *Fig. 9* shows that most of the radiometric impact of the side switch is observed over the SWIR band (<0.1K). When comparing $\bar{\delta}$ and $\bar{\delta_1}$ over the MWIR band, no statistical difference is observed, indicating the radiometric consistency between the MWIR Side-1 and Side-2 performance, and demonstrating the effective instrument calibration performed after the successful recovery of the MWIR band. In general, those results show that the radiometric impact is statistically not significant and in agreement with the assessment results presented in this Section using other methodologies.

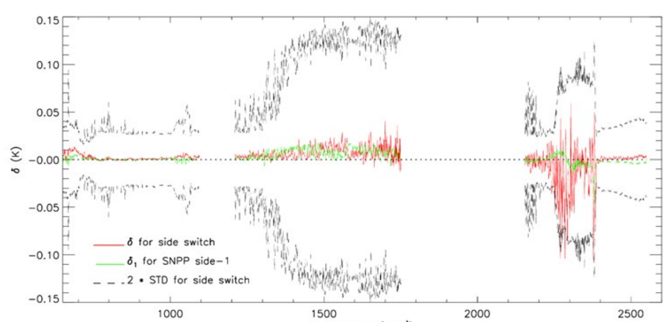

Fig. 9. The long-term effective radiometric impact of the SNPP CrIS side switch on the radiometric calibration performance (red-solid curve) and the corresponding standard deviation (black-dash curve), in brightness temperature, derived from daily radiometric comparisons between observations and simulations carried out within the August 15th to December 31st timeframe for the years 2018 (Side-1) and 2019 (Side-2). For comparison purposes, the radiometric differences found between two periods (September-October 2018 and November-December of 2018) when the instrument was operating under Side-1 electronics is reported (green-solid curve).

D. CrIS/IASI SNOs

Comparisons between the SNPP CrIS Side-1 and Side-2 radiometric performance were carried out using observations from the MetOp-B IASI as the radiometric transfer reference. The IASI instrument [10] on MetOp-B is a stable and well-

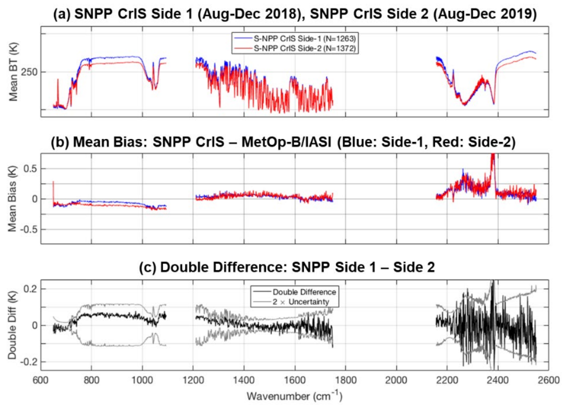

Fig. 10. The (a) SNPP CrIS mean brightness temperatures and (b) mean brightness temperature differences between SNPP CrIS Side-1 and MetOp-B IASI (blue-curve) and SNPP CrIS Side-2 and MetOp-B IASI (red curve), as well as (c) the double difference between Side-1 and Side-2 with the 2σ uncertainty (black and gray curves, respectively) for daytime observations (solar zenith angle greater than 95 degrees).

calibrated hyperspectral infrared sounder with no spectral gaps and finer spectral resolution compared to CrIS. Thus, the IASI spectra can easily be deconvolved onto the CrIS spectral grid to make a direct comparison. Additionally, since SNPP is in the mid-afternoon orbit and MetOp-B is in a mid-morning orbit, each with different altitudes, the CrIS and IASI sensor will view the same scene within a short interval of time during the simultaneous nadir overpasses (SNOs) of the two satellite platforms. Comparisons made during SNOs are a well-established technique for comparing two radiometers [11]. By comparing both Side-1 and Side-2 to MetOp-B IASI, radiometric differences between Side-1 and Side-2 can found via the double difference method. If properly applied, the method is expected to cancel out the MetOp-B IASI transfer reference. SNOs between SNPP CrIS and MetOp-B IASI occur roughly every 50 days. When that happens the SNOs last several days and occur for each orbit. SNOs are limited to the polar regions. Within the vicinity of the SNO, pairs of CrIS FOVs are spatially matched with IASI FOVs based on the following criteria: 1) FOVs within 13 km of one another and time difference of less than 2 minutes, and 2) the ratio of cosines of the satellite zenith angle for each FOV pair is less than 0.1. Finally, to limit errors due to collocation uncertainties, only homogeneous FOVs are considered. The scene homogeneity is assessed by collocating SNPP VIIRS pixels within each CrIS FOV. Only CrIS FOVs for which the coefficient of variation (ratio of the sample standard deviation to the mean) of the M16 VIIRS band is less than 0.05 are retained [12]. *Fig. 10* shows the results of the CrIS/IASI intercomparison for daytime observations. The Side-1 SNOs occurred between August and December of 2018 and Side-2 SNOs occurred between August and December of 2019. *Fig. 10(a)* shows the mean brightness temperatures for the Side-1 CrIS FOVs and the Side-2 CrIS FOVs. Similarly, *Fig. 10(b)* shows the mean biases between CrIS and IASI FOV pairs. *Fig. 10(c)* depicts the impact of the instrument side switch by means of the double difference between Side-1 and Side-2. These results show that the radiometric differences between Side-2 and Side-1 are within ±0.1K for the LWIR and MWIR band, and smaller than ±0.2K for nearly all channels over the SWIR band. Those radiometric changes are not statistically significant, since they are within the statistical uncertainty. The larger uncertainty observed in the SWIR band is mainly associated with the cold scene temperatures observed at the CrIS/IASI SNO location, which occur over the polar regions.

E. CrIS/AIRS SNOs

The SNO comparison between SNPP CrIS at full spectral resolution and the AIRS on-board the NASA's Earth Observing System Aqua spacecraft [13] were also carried out to evaluate the impact of the SNPP CrIS side switch. In contrast to the comparisons against IASI, AIRS comparisons are not limited to polar region domains and allow comparisons over a larger dynamic range of scene observations. With respect to the spatial and temporal matchup criteria, the CrIS and AIRS intercomparison is based on SNO locations that occur within a time difference of 12 minutes. The comparisons are restricted to near nadir observations. In this respect, only CrIS and AIRS observations that fall within an ellipse centered at the SNO with a minor axis of 75 km and with scan angles of less than 10° have been used. For CrIS, this corresponds to near nadir observations made at FORs 13, 14, 15 and 16, 17, 18. The scan angle difference between CrIS and AIRS is set to less than 3°. Thus, only observations where AIRS scan angles are within 3° of CrIS mean SNO angle are selected. The comparisons were limited to latitudes within ±40°. In order to assess scene homogeneity, only matchups where the standard deviation of the AIRS radiance at 900 cm^{-1} is less than 1 $mW/(m^2\ sr\ cm^{-1})$ are kept.

AIRS L1C v6.1 data was used in this analysis but only for the L1B channel set. The AIRS spectral response functions were applied to oversampled CrIS observations in order to map the CrIS data onto the AIRS spectral grid. However, since the AIRS grating has a variable spectral resolution in the wavenumber domain, a heavy spectral smoothing was applied to degrade the CrIS minus AIRS brightness temperature differences. CrIS/AIRS SNOs were collected for two periods, from July to December 2018 and July to December 2019, which correspond to six months of data of the SNPP CrIS instrument operating under Side-1 and Side-2 electronics, respectively.

Using the AIRS observations as the radiometric transfer reference, the radiometric impact of the CrIS side switch was determined by applying the double difference approach over the two periods where large ensemble of CrIS/AIRS SNOs were collected. Following the robust methodology described in [14, 15], the radiometric difference between the CrIS and AIRS observations corresponds to a weighted mean difference, where the weights are defined by the inverse of the spatial variance within each big circle SNO. The uncertainty in the weighted mean differences is also estimated. *Fig. 11* shows the AIRS mean brightness temperature, and the mean radiometric bias between CrIS and AIRS for the July-December period in 2018 and 2019. The bottom plot of *Fig. 11* reports the radiometric impact associated with the instrument side switch in the form of the double difference, with AIRS as the transfer reference. These results show that most of the radiometric differences before and after the side switch are well within ±0.1 K for most CrIS channels, particularly over the LWIR and MWIR band and are well within the statistical uncertainty of the methodology. The largest change in the mean difference is found in the SWIR band over the cold scenes around the 2300 cm^{-1} which are sensitive to small radiance uncertainties. These results, based on long-term intercomparisons against AIRS observations, are in agreement with other results presented here that show that radiometric differences over the side switch are not statistically significant.

In general, the largest radiometric differences occur in the SWIR band. Since those differences occur where the signal-to-noise (SNR) is lower, this indicates that the differences are dominated by the noise (noise-limited) rather than to changes in the radiometric calibration. Based on the results derived from several long-term radiometric performance analyses regarding the CrIS Side-2 radiometric calibration, no reasons were identified to change the radiometric calibration coefficients or the corresponding estimate of on-orbit radiometric uncertainty. Therefore, the radiometric uncertainty and radiometric stability estimates for the Side-2 remain unchanged from Side-1, as shown in Table *3*. The less than 10 mK ICT temperature difference seen on-orbit, after switching from Side-1 to Side-2 electronics, is consistent with results observed in pre-launch TVAC External Calibration Target (ECT) data. In addition to that, the pre-launch ECT view data has also shown no changes in the nonlinearity performance from Side-1 to Side-2, which is consistent with the on-orbit results presented here. This is totally expected due to the fact that the instrument detectors and preamplifiers are not changed during the sensor side switch. The results reported in this section strongly indicate the high radiometric quality consistency between the SNPP CrIS Side-1 and Side-2 calibrated observations. Thus, no impact is expected in the products derived from the CrIS observations.

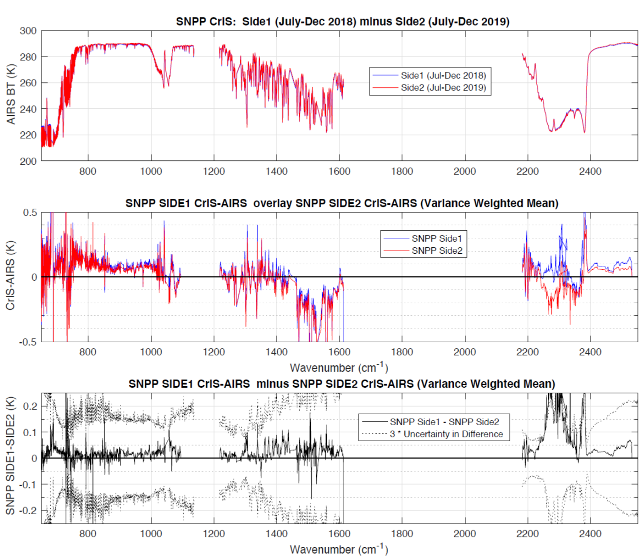

Fig. 11. Top: Plot of the mean brightness temperature spectra from July to December 2018 and July to December 2019. Middle: Overlay of mean CrIS minus AIRS brightness temperature for Side-1 and Side-2. Bottom: Double difference plot between CrIS Side-1 minus AIRS, and CrIS Side-2 minus AIRS.

IV. Radiometric Noise Assessment

The noise equivalent radiance differential (NEdN) estimates are reported as part of the CrIS SDR product. The NEdN

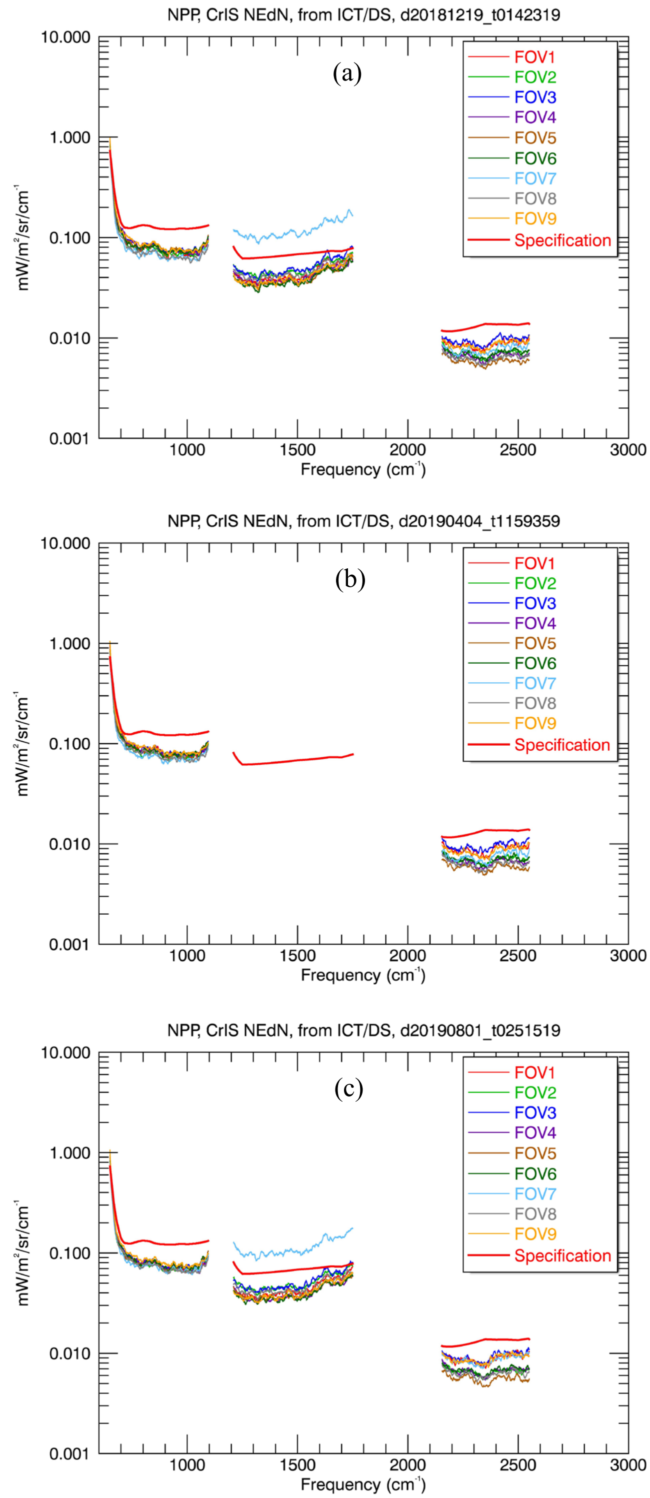

Fig. 12. Radiometric noise (NEdN) estimates (a) before the MWIR failure on 19 December 2018 (b) during the MWIR band anomaly on 4 April 2019 and (c) after the switch to Side-2 electronics on 1 August 2019.

calculation uses the on-board ICT, a high emissivity hot black body, and the deep space calibration views [16]. During the MWIR band failure, the NEdN was closely monitored. Fig. *12* shows the NEdN before (electronic Side-1), during (electronic Side-1), and after the MWIR failure (electronic Side-2). Overall, the NEdN changes were not significant from December 2018 to August 2019. *Fig. 13* shows the orbital mean percent change in NEdN between 15 August 2018 (electronic Side-1) and on 31 December 2019 (electronic Side-2). Only the SWIR FOV7 shows a noticeable noise increase of about 15%. In general, the NEdN change is within ±5%. In order to assess the long-term noise performance, *Fig. 14* shows the time series of the NEdN from 1 July 2019 to 30 June 2020. The LWIR FOV2 shows a noise increase on September 7 and 8 of 2019. The potential root source of this anomaly can likely be traced to a sudden electric charge and discharge in an electronic component linked to the LWIR FOV2 detector. Apart from this anomaly, the result presented in *Fig. 14* confirms the noise stability of the 27 SNPP CrIS FOVs and the noise consistency before and after the instrument side switch. Due to the importance of quantifying the instrument inter-channel noise correlations for weather forecast and environmental monitoring applications, *Fig. 15* reports the full correlation factor matrix representation of Side-1 and Side-2. This result helps to quantify the inter-channel noise correlation before and after the side switch. In general, no significant changes have been observed after the SNPP CrIS instrument was configured to operate using the Side-2 electronics.

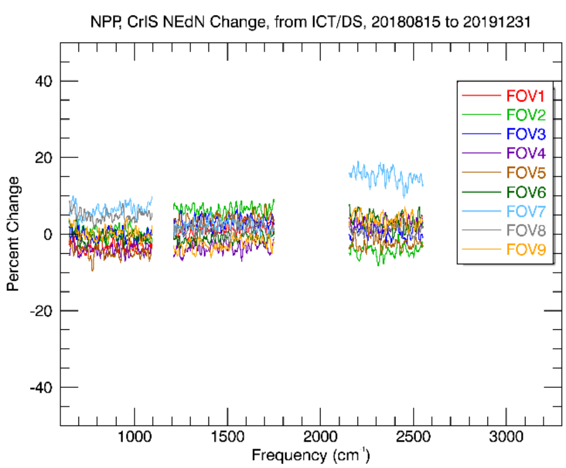

Fig. 13. Radiometric mean orbital NEdN percent change from 15 August 2018 (electronic Side-1) to 31 December 2019 (electronic Side-2).

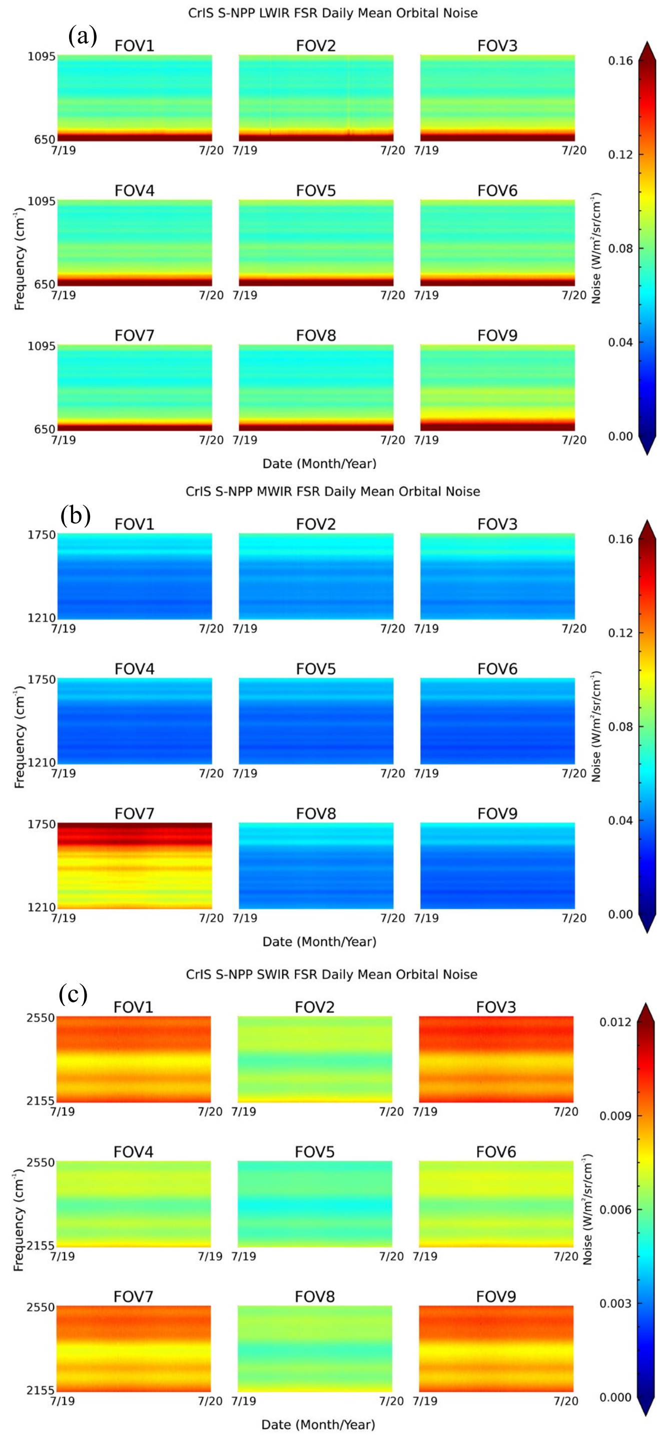

Fig. 14. Radiometric NEdN time series from 1 July 2019 to 30 June 2020 for the LWIR band (a), MWIR band (b), and the SWIR band (c).

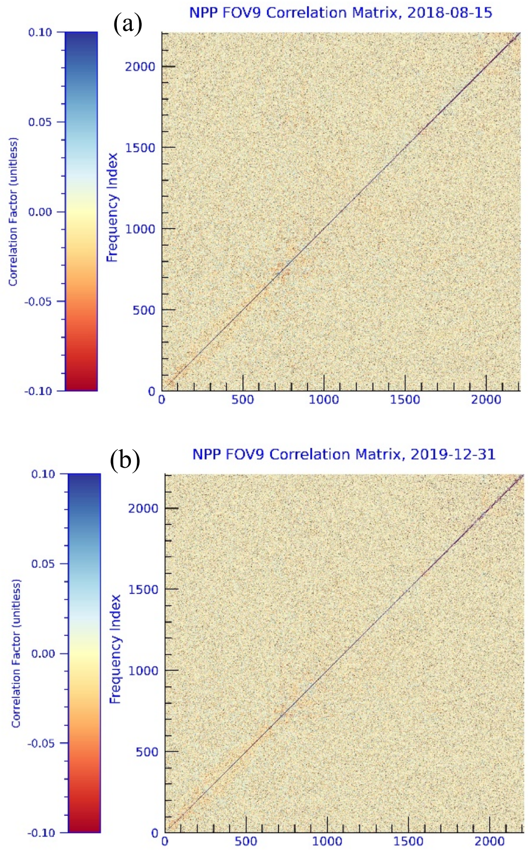

Fig. 15. CrIS SNPP FOV9 full correlation matrix on 15 August 2018 before the side switch (a) and on 31 December 2019 after the side switch (b).

V. Geolocation Calibration Assessment

After the instrument side switch, it was important to assess the quality of the geolocation of the CrIS SDR product due to its impact on the assimilation of SNPP CrIS radiances and in the generation of geophysical products that combine CrIS and ATMS observations. The geolocation calibration and the calculation of the SNPP CrIS SDR geolocation uncertainty makes use of the high spatial resolution (375 m) SNPP VIIRS I5 band observations that are spatially collocated and temporally coincident with the CrIS observations [17, 18]. For this purpose, the VIIRS I5 pixels observations are spatially averaged over the individual CrIS FOV footprint on the Earth surface. For the spectral matching between the CrIS and VIIRS observations, the CrIS hyperspectral observations in the LWIR band are multiplied and integrated with the VIIRS-I5 band spectral response function (SRF) and then normalized. This operation gives a single radiance value where its related brightness temperature is compared against the corresponding VIIRS brightness temperature. These steps allow the comparison of the CrIS and VIIRS observations.

For the geolocation calibration, the next step is to form a cost function based on an ensemble of the CrIS minus VIIRS differences. This cost function is minimized by shifting the VIIRS pixels location. The location of the best fit VIIRS pixel corresponds to the optimal latitude-longitude adjustment of the CrIS FOV center location. After a series of geometric transformations, this latter latitude-longitude adjustment is transformed into an adjustment of the commanded orientation angle of the CrIS instrument upfront pivoting mirror of the scene selection module (SSM) for both the in-track and cross-track directions. Using this process, for each of the 30 FOR scanning angles (index i), optimized cross-track ($\lambda_{cr,i}$) and in-track ($\lambda_{in,i}$) SSM angles are generated. This result in a total of 60 SSM angle values for a given orbit. An average over three days is used to generate the optimal set of these 60 SSM angles. Those optimal SSM angles are uploaded to the spacecraft within the engineering packet table, which is regularly downloaded as part of the sensor data stream, and utilized by the ground data processing to define the geolocation of the CrIS calibrated observations. It is important to mention that the geolocation calibration was performed only after the sensor spectral calibration was completed, since it includes new detector positions relative to the interferometer optical axis.

Using CrIS SDR data generated with the new set of optimized SSM angles, the assessment of the CrIS SDR geolocation is performed using the VIIRS-I5 observations as the geolocation reference. As part of this process, the SSM angle error in the cross-track ($\delta\lambda_{cr,i}$) and in-track ($\delta\lambda_{in,i}$) for each FOR scanning index i is calculated. By taking the contributions of the systematic and random components of the CrIS cross-track and in-track SSM angles errors, and the VIIRS geolocation uncertainty, the SNPP CrIS angular geolocation uncertainty for a given FOR ($\delta\lambda_{g,i}$) can be expressed as

$$\delta\lambda_{g,i} = \sqrt{\begin{array}{c}\left(\overline{\delta\lambda}_{cr,i}\right)^2 + \left(\overline{\delta\lambda}_{in,i}\right)^2 + VAR\left(\delta\lambda_{cr,i}\right) + VAR\left(\delta\lambda_{in,i}\right) \\ +[\tan^{-1}(\Delta\lambda_{VIIRS}/H)]^2\end{array}} \tag{3}$$

where the terms $\overline{\delta\lambda}_{cr,i}$ and $\overline{\delta\lambda}_{in,i}$ represent the systematic SSM angle errors in the cross-track and in-track directions, respectively, for a particular FOR. The terms $VAR\left(\delta\lambda_{cr,i}\right)$ and $VAR\left(\delta\lambda_{in,i}\right)$ are the variance of the SSM angle errors in the cross-track and in-track directions, respectively, representing the random error contributions. The last term of Equation (1) represents the contribution from the VIIRS geolocation angle uncertainty, where $\Delta\lambda_{VIIRS}$ represents the VIIRS geolocation uncertainty in meters, which is about 92 meters [19], and H represents the instrument mean altitude, which is approximately 824 km.

On 24 June 2019, the EP version 38 was uploaded containing the initial electronic Side-2 calibration coefficients. On 28 June 2019, the EP version 39 was uploaded, and it contained adjusted coefficients, such as the programmable gain amplifier tables, to optimize the instrument performance. The EP version 39 did not contain calibration adjustments for the instrument line shape (ILS) parameters nor the geolocation calibration. An offline intermediate SDR product data set was then generated using the EP version 39 modified with the new estimated ILS parameters. Using this intermediate SDR data set, the geolocation parameters were estimated and integrated into the EP version 40 that became operational on 1 August 2019. Fig. 16 shows a time series of the geolocation accuracy during the

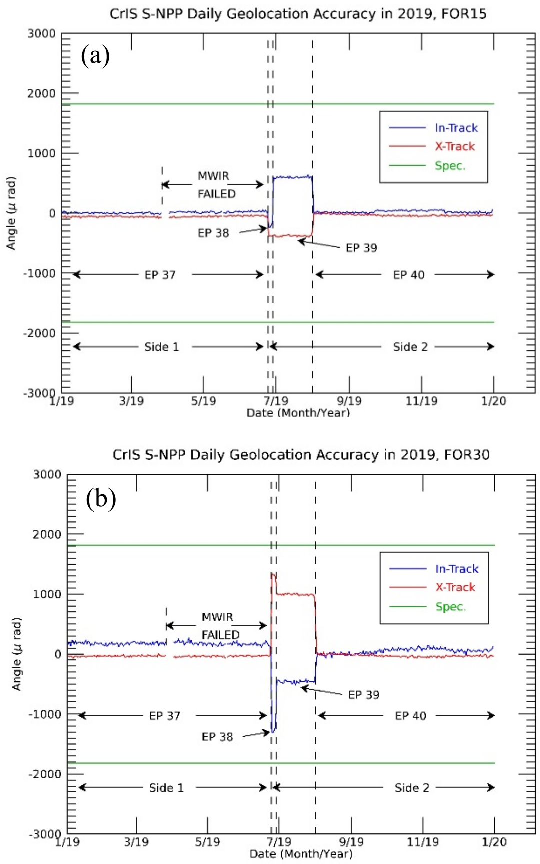

Fig. 16. SNPP CrIS SDR geolocation accuracy estimates for FOR 15 (a), and FOR 30 (b) during the year 2019.

year 2019 for FOR 30. The FOR 30 has the largest geolocation error compared to the other FORs. This could be associated with the footprint of the CrIS and VIIRS instruments that gets bigger at the highest cross-track location, where the match of these two footprints are not as good compared to the nadir location. However, additional assessment is needed to further understand this performance. For the period in which the instrument was operating using Side-1 electronics, the geolocation accuracy had a systematic bias of about 200 microradians (μrad) and it remained stable during the loss of the MWIR band. A large geolocation error was introduced during the operational use of the EP version 38 and 39 (electronic Side-2). After the upload of the EP version 40, the geolocation accuracy has improved with respect to the Side-1 performance and appears to have a seasonal variation on the order of 100 microradians. The geolocation accuracy of the CrIS SDR validated product is within 200 microradians, which corresponds to approximately 250 meters. This value is well below the JPSS Level-1 geolocation accuracy requirement (about 1.5 km). In order to further understand the long-term performance of the SNPP CrIS SDR geolocation and the impact of the side switch, Fig. *17* presents the geolocation accuracy estimates and the total SNPP CrIS SDR uncertainty as function the 30 FORs for two days with largest geolocation errors, one occurring six months before the MWIR band failure and another observed six months after the upload of the EP version 40. On 15 January 2019, the highest geolocation uncertainty occurred at the FOR 11. For this case, the total geolocation uncertainty amounts to 181 meters at the corresponding nadir location. On 12 November 2019, the highest geolocation uncertainty occurred for the FOR 29 amounting to 187 meters at the corresponding nadir location. These results show that the geolocation uncertainty meets the specification with margin both before the side switch and after the upload of the EP 40 for all FORs. However, the geolocation uncertainty is very high from 24 June 2019 to 1 August 2019 during the use of EP version 38 and 39.

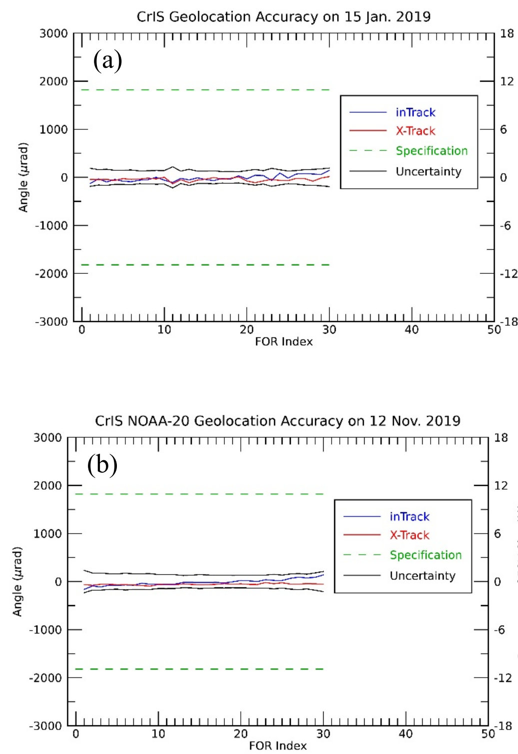

Fig. 17. SNPP CrIS SDR geolocation accuracy (in-track and cross-track) and the total geolocation uncertainty for the 30 Earth scenes FORs position on 15 January 2019 with the electronic Side-1 (a) and on 12 November 2019 with the electronic Side-2 (b).

VI. Impact and Benefits for Restoring the Full Capabilities of the SNPP CrIS Instruments

The operational assimilation of the first SNPP CrIS observations occurred just a few months after reaching the JPSS validated maturity level on 31 January 2013 at the NOAA National Weather Service (NWS)/National Centers for Environmental Prediction (NCEP). The efforts to assess the impact of the SNPP CrIS data started on 20 Aug 2012 [20], while its assimilation as part of the operational Global Forecast System (GFS) took place on 20 August 2013, when implemented in the Global Data Assimilation System (GDAS) [21] at 1200 UTC. At the United Kingdom Meteorological Office (Met Office), the assimilation of the SNPP CrIS radiances became operational on 30 April 2013 [22]. At the European Centre for Medium-range Weather Forecasts (ECMWF) the operational assimilation started with 78 CrIS channels on 22 January 2015. Later, on 22 November 2016, the number of assimilated CrIS channels was increased to 117 [23], and further to 118 on 11 July 2017.

The impact of the loss of the SNPP CrIS observations on headline NWP forecast scores is presented in *Fig. 18*, including the forecast impact of losing only the SNPP CrIS MWIR band. The major forecast impact associated with the lack of access to SNPP CrIS radiances occurred over the North Hemisphere at forecast days 3 and 5. The analysis also shows that no statistically significant impact is observed from losing only the SNPP CrIS MWIR band. *Fig. 18* results do not account for NOAA-20 CrIS observations, however, the weather forecast impact during the loss of the SNPP CrIS MWIR band was mainly mitigated due to the redundancy provided by NOAA-20 CrIS radiances. Both SNPP and NOAA-20 occupy the same orbit with half-orbit (about 50 min) separation. NOAA-20 was designated as the primary afternoon (PM) satellite during the week of 11 February 2019, about one month before the failure of the SNPP CrIS MWIR band. By this time, the NOAA-20 CrIS SDR product had already reached the JPSS validated maturity level on 14 August 2018.

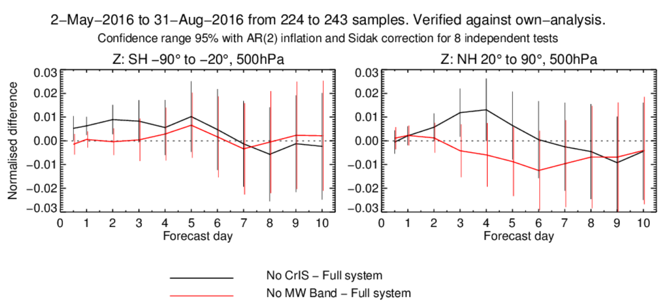

Fig. 18. Forecast impact of the denial of all SNPP CrIS radiances at NSR in the ECMWF NWP system (black-line) verified against ECMWF analysis. The red-line result corresponds to the loss of the SNPP CrIS MWIR band. Positive values indicate forecast skill degradation due to using less data. The SNPP CrIS data is from 2 May 2016 to 31 August 2016.

The loss of the SNPP CrIS MWIR band signified the loss of channels sensitive to atmospheric water vapor. However, the major impact of the assimilated CrIS observations comes from LWIR channels which are critical for providing tropospheric and lower stratospheric temperature information. Compared to the LWIR temperature channels, only a few MWIR channels sensitive to water vapor were assimilated at ECMWF at the time preceding the loss of the SNPP CrIS MWIR band. The NWP operational systems are highly resilient systems that rely on a robust and diverse global observing system [24] to obtain global temperature and water vapor information. This includes microwave and infrared observations from operational polar-orbiting and geostationary satellites that form part of the Environmental Observation Satellite network.

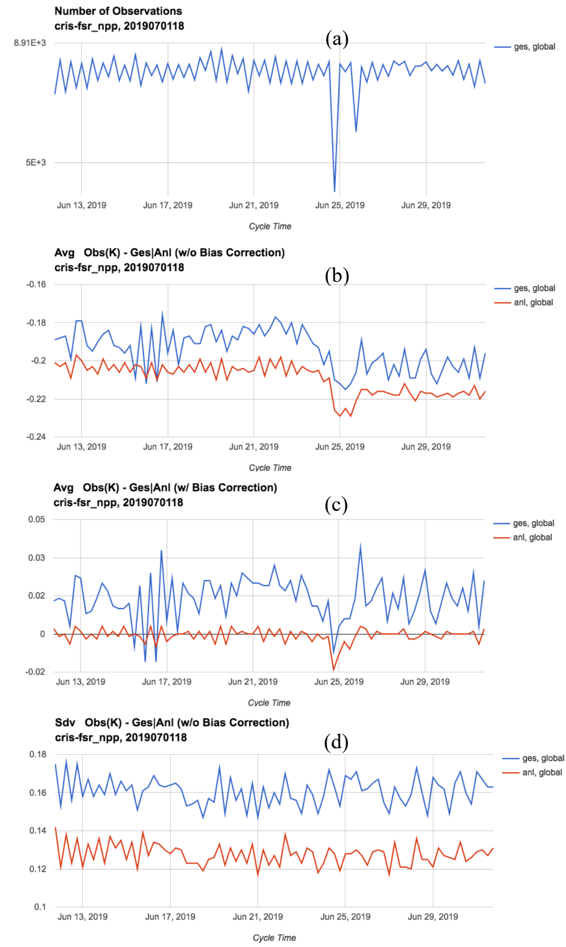

Fig. 19. The effects of the SNPP CrIS side switch on the (a) number of assimilated observations and on the mean departure between observed SNPP CrIS Side-2 brightness temperatures and simulated brightness temperatures from the six-hour forecast, or "guess", (blue-line) and the analysis fields (red-line) through the side transition (b) before and (c) after bias correction at channel 91 (706.25 cm^{-1}) in the NOAA/NCEP operational data assimilation system. The standard deviation of the departures before bias correction is shown in (d).

After the recovery of the MWIR band, and the full recalibration of the SNPP CrIS sensor, the quality and impact of SNPP CrIS SDR Side-2 product was assessed within the NCEP and ECMWF systems. Some results provided by those institutions are presented in this section. The effects of the SNPP side switch on the NOAA/NCEP operational data assimilation system are presented in *Fig. 19*. *Fig. 19(a)* illustrates the impact in the number of assimilated observations around the instrument side switch for the lowest-noise channel (706.25 cm^{-1}). A reduction in the number of assimilated observations is clearly observed during the actual switch to the redundant electronics on 24 June 2019. A few days after this event, the number of observations became stable and nearly at the same level as before the instrument side switch. This is particularly evident on 28 June 2019, when the quality of the Side-2 SDR data reached the provisional maturity level. This result suggests that changes in the quality of the SNPP CrIS radiances were captured by the data assimilation quality control. *Fig. 19(b)-(c)* show the mean departure between observed and simulated SNPP CrIS brightness temperatures before and after bias correction through the side transition. A small change in bias of ~0.02 K is seen in the uncorrected bias following the side switch. These results show how the system reacted to a small bias change when the side switch occurred. The bias correction adapts immediately after the instrument side switch to compensate. As shown in *Fig. 19(d)*, the standard deviation did not significantly change suggesting no significant change in the quality of the data from switching sides. After the instrument transition, NCEP reported that the observations from MWIR band were available with reasonable statistics (not presented here). Presently, eight MWIR band channels, sensitive to water vapor, are assimilated at NCEP.

Further assessment of the quality of the SNPP CrIS SDR Side-2 product was carried out by observing the impact on the Observation minus Background (O-B) statistics for selected SNPP CrIS channels before and after the instrument side switch. This task was performed at ECMWF by computing the standard deviation of the departure of SNPP CrIS over the last 47 days of 2018 (Side-1) and 2019 (Side-2), which are presented in *Fig. 20*. These results are normalized by the standard deviation of the O-B of NOAA-20 CrIS SDR in order to identify any change in noise in the LWIR band of the SNPP CrIS SDR Side-2 products. By observing the results in *Fig. 20*, it is clear that no significant statistically differences are identified after the SNPP CrIS side switch, confirming the consistency between the Side-1 and Side-2 SDR products. At ECMWF, the number of assimilated CrIS MWIR band channels increased from 7 to 37. This happened on 14 November 2019 for NOAA-20 and on 15 September 2020 for SNPP. Both of these changes were backed up by positive forecast impact in experimental suites. The combined use of LWIR and MWIR bands now totals 148 channels from each CrIS instrument onboard SNPP and NOAA-20 satellites.

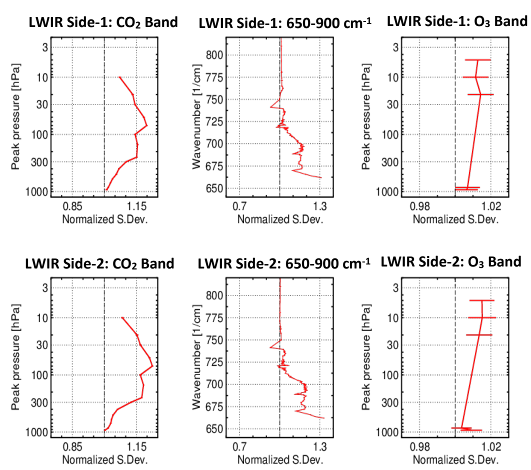

Fig. 20. Standard deviation of the Observation minus Background (O-B) departure of SNPP CrIS in the last 47 days of 2018 (top) and 2019 (bottom), normalized by the standard deviation of the O-B of NOAA-20 CrIS. The peak pressure in the CO_2 and O_3 sounding channel figures refer to the level at which each channel's weighting function has the maximum value. The wavenumber-space figures contain all channels in the range 650-900 cm^{-1}, but no O_3 channels.

Due to the recent recovery of the SNPP CrIS instrument and the demonstrated high quality of the CrIS calibrated observations, presently, the SNPP CrIS observations are being assimilated at operational NWP centers and used in near real-time by Direct Broadcast (DB) users to support their forecast capabilities. In addition to that, it is possible to take advantage of the spatial and temporal coverage resulted from combining SNPP and NOAA-20 CrIS observations. In regions with nearly clear-sky conditions, there is higher value of CrIS observations, due to the fact that more observations will pass the quality control during the assimilation process. During the very active 2020 Atlantic hurricane season, the CrIS observations from the SNPP and NOAA-20 CrIS instruments were assimilated by NWP centers. *Fig. 21* shows that by combining the hyperspectral infrared observations from the two on-orbit CrIS instruments observation gaps are reduced resulting in improved spatial coverage.

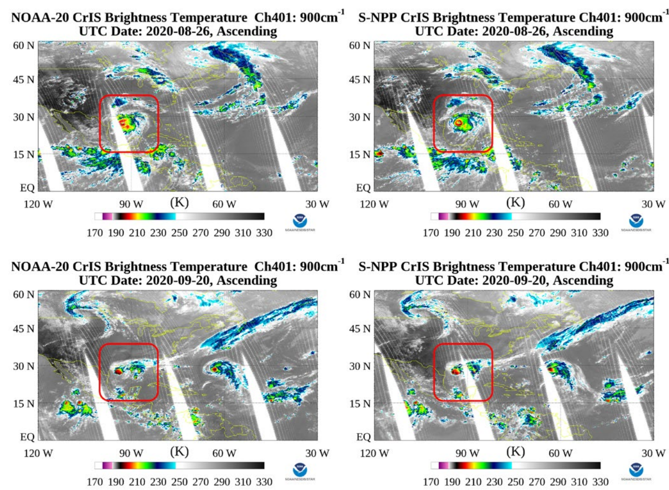

Fig. 21. CrIS observations from NOAA-20 (left) and SNPP (right) at 900 cm^{-1} during the development of the tropical cyclone Laura (top), on 26 August 2020, and Beta/Teddy (bottom) on 20 September 2020. As shown inside the red-rectangles, combining CrIS observations helps to reduce observation gaps and increases the temporal resolution of Earth observation.

The other major application for the CrIS instrument is the NOAA-Unique Combined Atmospheric Processing System (NUCAPS). The CrIS instrument is used in conjunction with the Advanced Technology Microwave Sounder (ATMS) observations to derive environmental data record (EDR) products over all-weather conditions, providing nearly global coverage. The CrIS observations are acquired at a critical time for the evaluation of the thermodynamic conditions of severe weather. Of particular interests are observation in the early afternoon, given that this is typically the time-frame of the initiation of convection. NUCAPS CrIS/ATMS soundings have demonstrated value in the detection of cold air aloft in Alaska [25, 26], characterizing the pre-convective environment to improve forecasts of severe weather [27-29], improving the tropical cyclone forecasts [30], and air quality forecasts using sounder-derived ozone [31] and carbon monoxide retrievals

[32]. Typically, forecasters require soundings in the most difficult scenes. With the loss of the SNPP midwave band the NUCAPS water vapor retrievals were degraded, both in global coverage and skill. While ATMS did provide the necessary information content to provide reasonable EDRs, the SNPP product was shown to be measurably different than the NOAA-20 product. Figure 22 shows an example of the NUCAPS total precipitable water vapor product, derived using CrIS and ATMS observations from the SNPP and NOAA-20 satellites. In this figure it can be seen that SNPP complements the observations of NOAA-20 in that when there is an orbital gap or edge of scan observations in one satellite the other satellite is viewing at nadir. Subtle differences are also seen over the 50-minute difference in observation time. Having a fully functional CrIS instrument on both satellites allows us to attribute these differences to changes in meteorology rather than algorithm changes due to the instrument spectral coverage.

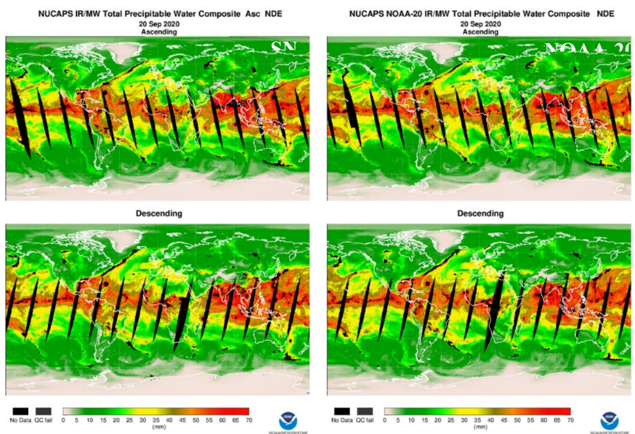

Fig. 22. NUCAPS SNPP (left) and NOAA-20 (right) Total Precipitable Water Vapor derived from CrIS and ATMS observations on 20 September 2020, during the 2020 hurricane season. Those products hold similar quality over global scale and benefit from the high quality and consistency of the CrIS and ATMS.

VII. Conclusion

The JPSS Missions Operations Team (MOT) successfully switched the SNPP CrIS from primary to redundant side electronics without major issues. Full performance was restored following the side switch, with redundant side performance being comparable to that on the primary side. Even though critical calibration electronics, including the ICT temperature sensors, reside in the redundant circuitry, both sides had been thoroughly checked out during ground testing and calibration constants for both sides were available at launch. The availability of this information was key for the successful instrument restoration. The engineering packet parameters for the redundant side were adjusted after the switch to optimize SDR continuity over absolute accuracy. However, it is important to highlight that the difference between optimizing continuity versus accuracy is very small. This manuscript demonstrates the high quality of the SNPP CrIS SDR Side-2 product after the full restoration and recalibration of the SNPP CrIS instrument. The long-term radiometric assessment of the SNPP CrIS SDR Side-2 product includes radiometric inter-comparisons against SNPP/VIIRS, MetOp-B/IASI, Aqua/AIRS and NOAA-20/CrIS observations as well as simulated radiances. The evaluation of the spectral quality of the SDR product was mainly based on simulated observations, while the geolocation quality of the CrIS SDR product was assessed using the high spatial resolution and accurate geolocation of the SNPP VIIRS observations. The SNPP CrIS SDR products have been reliably produced by IDPS since the transition to Provisional Maturity on 1 August 2019. Derived from this intensive evaluation and monitoring, following assessments of the SNPP CrIS instrument and SDR Side-2 product are given:

1. The spectral offsets among the 9 FOVs for all three bands is within ±2.5 ppm;
2. The radiometric FOV-to-FOV consistency is within 0.1 K;
3. The on-orbit NEdN for all FOVs and bands are within the specification (MW FOV7 is out of family as before side switch) and comparable to SNPP CrIS Side-1;
4. The in-track and cross-track geolocation uncertainty is within 200 meters, relative to SNPP VIIRS, for all FORs;
5. The rate of good data quality after instrument side switch is greater than 99.7%, which is the same as Side-1 data quality rate.

The quality of the SNPP CrIS SDR Side-2 product is sufficient to be used in operational environments as confirmed by inputs from NOAA/NWS/NCEP, ECMWF and the Naval Research Laboratory (NRL). Weather forecast centers are planning on increasing the number of MWIR band channels, due to the favorable impact of assimilating channels sensitive to tropospheric water vapor. ECMWF has already increased from 7 to 37 the number of assimilated CrIS MWIR channels for both NOAA-20 and SNPP. Major observations derived from the assessment of the SNPP CrIS SDR product are listed below:

1. The long-term statistical performance of the difference between observations and background, monitored at NWP centers, confirmed the consistent and stable quality of the SNPP CrIS SDR data before and after the side switch;
2. No identifiable changes were observed in the standard deviation of O-B over the assimilated SNPP CrIS Side-2 observations. The standard deviation is within the expected NWP errors;
3. The overall observed impact for SNPP CrIS observations is still consistently positive, with no issues of concern. No adjustments to the quality control or observation error were needed to accommodate the impact of the side switch. The SNPP CrIS sensor continues to provide benefits to the NWP skill;

Takeaways from this work are not only around the importance and benefits of the CrIS instrument design redundancy, but also around the lessons learned during the switch to Side-2 electronics. Those lessons will be relevant to respond with more efficiency and promptitude during a similar event found within the CrIS program in the future. Examples of lessons learned include the needed improvements to the process for transferring updates to the initial geolocation parameters from the primary to the redundant side. The first guess for the on-orbit redundant side geolocation parameters was not optimal, and the subsequent update for the in-track torque null position made the SNPP CrIS SDR geolocation worse instead of better. In addition to that, it is critical to maintain up to date configuration files for both primary and redundant sides and the instrument activation procedures for the redundant side.

The excellent performance of the CrIS sensors on SNPP and NOAA-20 will continue with the JPSS-2 CrIS sensor, planned to be deployed into space around September 2022. In this regard, a constellation of CrIS sensors will provide continuity, redundancy and will enhance critical capabilities needed for numerical weather forecasting and environmental monitoring.

Acknowledgment

The authors would like to thank the NOAA-NASA Operations team, including Michael Stager, Greg Privette, Jodi Vezzetti, Sarah Riley and Lori Spalsbury, the Harris team, including Don Ripplinger, Sara Glass and Jeff Garr, the NOAA Products Validation System (NPROVS) team, including Tony Reale and Bomin Sun, the NUCAPS Team, including Nick Nalli, Changyi Tan, Murty Divakarla, and Ken Pryor as well as Mitch Goldberg, Lihang Zhou, Satya Kalluri and Changyong Cao for their great support during the SNPP CrIS restoration activities.

References

[1] Y. Han, H. Revercomb, M. Cromp, D. G. Gu, D. Johnson, D. Mooney, D. Scott, L. Strow, G. Bingham, L. Borg, Y. Chen, D. DeSlover, M. Esplin, D. Hagan, X. Jin, R. Knuteson, H. Motteler, J. Predina, L. Suwinski, J. Taylor, D. Tobin, D. Tremblay, C. M. Wang, L. H. Wang, L. K. Wang, and V. Zavyalov, "Suomi NPP CrIS measurements, sensor data record algorithm, calibration and validation activities, and record data quality," (in English), *Journal of Geophysical Research-Atmospheres,* vol. 118, no. 22, pp. 12734-12748, Nov 27 2013.

[2] Y. Han and Y. Chen, "Calibration Algorithm for Cross-Track Infrared Sounder Full Spectral Resolution Measurements," (in English), *Ieee Transactions on Geoscience and Remote Sensing,* vol. 56, no. 2, pp. 1008-1016, Feb 2018.

[3] L. L. Strow, S. E. Hannon, S. De Souza-Machado, H. E. Motteler, and D. Tobin, "An overview of the AIRS radiative transfer model," (in English), *Ieee Transactions on Geoscience and Remote Sensing,* vol. 41, no. 2, pp. 303-313, Feb 2003.

[4] L. L. Strow, H. Motteler, D. Tobin, H. Revercomb, S. Hannon, H. Buijs, J. Predina, L. Suwinski, and R. Glumb, "Spectral calibration and validation of the Cross-track Infrared Sounder on the Suomi NPP satellite," (in English), *Journal of Geophysical Research-Atmospheres,* vol. 118, no. 22, pp. 12486-12496, Nov 27 2013.

[5] Y. Chen, Y. Han, and F. Z. Weng, "Characterization of Long-Term Stability of Suomi NPP Cross-Track Infrared Sounder Spectral Calibration," (in English), *Ieee Transactions on Geoscience and Remote Sensing,* vol. 55, no. 2, pp. 1147-1159, Feb 2017.

[6] D. Tobin, H. Revercomb, R. Knuteson, J. Taylor, F. Best, L. Borg, D. DeSlover, G. Martin, H. Buijs, M. Esplin, R. Glumb, Y. Han, D. Mooney, J. Predina, L. Strow, L. Suwinski, and L. K. Wang, "Suomi-NPP CrIS radiometric calibration uncertainty," (in English), *Journal of Geophysical Research-Atmospheres,* vol. 118, no. 18, pp. 10589-10600, Sep 27 2013.

[7] *Validated Maturity Science Review for NOAA-20 CrIS SDR, October 2, 2018. [Online].* . Available: https://www.star.nesdis.noaa.gov/jpss/documents/AMM/N20/CrIS_SDR_Validated.pdf

[8] L. K. Wang, M. Goldberg, X. Q. Wu, C. Y. Cao, R. A. Iacovazzi, F. F. Yu, and Y. P. Li, "Consistency assessment of Atmospheric Infrared Sounder and Infrared Atmospheric Sounding Interferometer radiances: Double differences versus simultaneous nadir overpasses," (in English), *Journal of Geophysical Research-Atmospheres,* vol. 116, Jun 8 2011.

[9] A. P. McNally and P. D. Watts, "A cloud detection algorithm for high-spectral-resolution infrared sounders," (in English), *Quarterly Journal of the Royal Meteorological Society,* vol. 129, no. 595, pp. 3411-3423, Oct 2003.

[10] F. Hilton, R. Armante, T. August, C. Barnet, A. Bouchard, C. Camy-Peyret, V. Capelle, L. Clarisse, C. Clerbaux, P. F. Coheur, A. Collard, C. Crevoisier, G. Dufour, D. Edwards, F. Faijan, N. Fourrie, A. Gambacorta, M. Goldberg, V. Guidard, D. Hurtmans, S. Illingworth, N. Jacquinet-Husson, T. Kerzenmacher, D. Klaes, L. Lavanant, G. Masiello, M. Matricardi, A. McNally, S. Newman, E. Pavelin, S. Payan, E. Pequignot, S. Peyridieu, T. Phulpin, J. Remedios, P. Schlussel, C. Serio, L. Strow, C. Stubenrauch, J. Taylor, D. Tobin, W. Wolf, and D. Zhou, "HYPERSPECTRAL EARTH OBSERVATION FROM IASI Five Years of Accomplishments," (in English), *Bulletin of the American Meteorological Society,* vol. 93, no. 3, pp. 347-370, Mar 2012.

[11] C. Y. Cao, M. Weinreb, and H. Xu, "Predicting simultaneous nadir overpasses among polar-orbiting meteorological satellites for the intersatellite calibration of radiometers," (in English), *Journal of Atmospheric and Oceanic Technology,* vol. 21, no. 4, pp. 537-542, Apr 2004.

[12] L. Wang, Y. Han, X. Jin, Y. Chen, and D. A. Tremblay, "Radiometric consistency assessment of hyperspectral infrared sounders," (in English), *Atmospheric Measurement Techniques,* vol. 8, no. 11, pp. 4831-4844, 2015.

[13] M. T. Chahine, T. S. Pagano, H. H. Aumann, R. Atlas, C. Barnet, J. Blaisdell, L. Chen, M. Divakarla, E. J. Fetzer, M. Goldberg, C. Gautier, S. Granger, S. Hannon, F. W. Irion, R. Kakar, E. Kalnay, B. H. Lambrigtsen, S.-Y. Lee, J. Le Marshall, W. W. McMillan, L. McMillin, E. T. Olsen, H. Revercomb, P. Rosenkranz, W. L. Smith, D. Staelin, L. L. Strow, J. Susskind, D. Tobin, W. Wolf, and L. Zhou, "Airs," *Bulletin of the American Meteorological Society,* vol. 87, no. 7, pp. 911-926, 2006.

[14] D. Tobin, H. Revercomb, B. Knuteson, F. Best, J. Taylor, D. Deslover, L. Borg, C. Moeller, G. Martin, R. Kuehn, G. Quinn, and R. Garcia, "Soumi NPP/JPSS Cross-Track Infrared Sounder (CrIS): Intercalibration with AIRS, IASI, and VIIRS," in *The 93rd AMS Annual Meeting*, Austin, Texas, USA, 2013.

[15] D. Tobin, R. Holz, F. Nagle, and H. Revercomb, "Characterization of the Climate Absolute Radiance and Refractivity Observatory (CLARREO) ability to serve as an infrared satellite intercalibration reference," (in English), *Journal of Geophysical Research-Atmospheres,* vol. 121, no. 8, pp. 4258-4271, Apr 27 2016.

[16] (2018). *Joint polar satellite system (JPSS) Cross Track Infrared Sounder (CrIS) sensor data records (SDR) algorithm theoretical basis document (ATBD) for full spectral resolution*. Available: https://www.star.nesdis.noaa.gov/jpss/Docs.php

[17] L. K. Wang, D. A. Tremblay, Y. Han, M. Esplin, D. E. Hagan, J. Predina, L. Suwinski, X. Jin, and Y. Chen, "Geolocation assessment for CrIS sensor data records," (in English), *Journal of Geophysical Research-Atmospheres,* vol. 118, no. 22, pp. 12690-12704, Nov 27 2013.

[18] L. K. Wang, B. Zhang, D. Tremblay, and Y. Han, "Improved scheme for Cross-track Infrared Sounder geolocation assessment and optimization," (in English), *Journal of Geophysical Research-Atmospheres,* vol. 122, no. 1, pp. 519-536, Jan 2017.

[19] R. E. Wolfe, G. Q. Lin, M. Nishihama, K. P. Tewari, J. C. Tilton, and A. R. Isaacman, "Suomi NPP VIIRS prelaunch and on-orbit geometric calibration and characterization," (in English), *Journal of Geophysical Research-Atmospheres,* vol. 118, no. 20, pp. 11508-11521, Oct 27 2013.

[20] J. G. Yoe, "Using Satellite Sounder Observations at NCEP and Future Plans," in *Community Meeting on NOAA Satellites*, 2020.

[21] E. M. Center, K. Campana, P. Caplan, D. J. Halperin, B. Lapenta, S. Lilly, Y. Lin, A. B. Penny, S. Saha, V. Tallapragada, G. H. White, J. S. Woollen, and F. Yang, "The Development and Success of NCEP's Global Forecast System," in *99th American Meteorological Society Annual Meeting*, Phoenix, Arizona, 2019.

[22] A. Smith, N. Atkinson, W. Bell, and A. Doherty, "An initial assessment of observations from the Suomi-NPP satellite: data from the Cross-track Infrared Sounder (CrIS)," (in English), *Atmospheric Science Letters,* vol. 16, no. 3, pp. 260-266, Jul-Sep 2015.

[23] R. Eresmaa, J. Letertre-Danczak, C. Lupu, N. Bormann, and A. P. McNally, "The assimilation of Cross-track Infrared Sounder radiances at ECMWF," (in English), *Quarterly Journal of the Royal Meteorological Society,* vol. 143, no. 709, pp. 3177-3188, Oct 2017.

[24] W. Programmes. (April 1, 2021). *Global Observing System*. Available: https://public.wmo.int/en/programmes/global-observing-system

[25] R. Esmaili, N. Smith, M. Schoeberl, and C. Barnet, "Evaluating Satellite Sounding Temperature Observations for Cold Air Aloft Detection," (in English), *Atmosphere,* vol. 11, no. 12, p. 1360, Dec 2020.

[26] G. M. Weaver, N. Smith, E. B. Berndt, K. D. White, J. F. Dostalek, and B. T. Zavodsky, "Addressing the Cold Air Aloft Aviation Challenge with Satellite Sounding Observations," *Journal of Operational Meteorology,* vol. 3, no. 1, pp. 138-152, 2019.

[27] F. Iturbide-Sanchez, S. R. S. da Silva, Q. H. Liu, K. L. Pryor, M. E. Pettey, and N. R. Nalli, "Toward the Operational Weather Forecasting Application of Atmospheric Stability Products Derived From NUCAPS CrIS/ATMS Soundings," (in English), *Ieee Transactions on Geoscience and Remote Sensing,* vol. 56, no. 8, pp. 4522-4545, Aug 2018.

[28] R. B. Esmaili, N. Smith, E. B. Berndt, J. F. Dostalek, B. H. Kahn, K. White, C. D. Barnet, W. Sjoberg, and M. Goldberg, "Adapting Satellite Soundings for Operational Forecasting within the Hazardous Weather Testbed," (in English), *Remote Sensing,* vol. 12, no. 5, p. 886, Mar 2020.

[29] N. Smith, K. D. White, E. Berndt, B. T. Zavodsky, A. Wheeler, M. A. Bowlan, and C. D. Barnet, "NUCAPS in AWIPS – rethinking information compression and distribution for fast decision making," in *22nd AMS Conf. on Sat. Meteor. & Ocean*, Austin, TX 2018, vol. 6a.6, p. 4 pages.

[30] E. Berndt, N. Smith, J. Burks, K. White, R. Esmaili, A. Kuciauskas, E. Duran, R. Allen, F. LaFontaine, and J. Szkodzinski, "Gridded Satellite Sounding Retrievals in Operational Weather Forecasting: Product Description and Emerging Applications," (in English), *Remote Sensing,* vol. 12, no. 20, p. 3311, Oct 2020.

[31] E. B. Berndt, B. T. Zavodsky, and M. J. Folmer, "Development and Application of Atmospheric Infrared Sounder Ozone Retrieval Products for Operational Meteorology," (in English), *Ieee Transactions on Geoscience and Remote Sensing,* vol. 54, no. 2, pp. 958-967, Feb 2016.

[32] N. Smith, R. Esmaili, C. D. Barnet, G. Frost, S. A. McKeen, M. Trainer, and C. Francoeur, "Monitoring atmospheric composition and long-range smoke transport with NUCAPS satellite soundings in field campaigns and operations," in *AMS 100th Annual Meeting*, Boston, MA, 2020, vol. 2B.6, p. 5 pgs.

Flavio Iturbide-Sanchez (S'03–M'07–SM'19) received the B.S.E.E degree in electronics engineering from Autonomous Metropolitan University, Mexico City, Mexico, in 1999, the M.S.E.E. degree in electrical engineering from the Advanced Studies and Research Center, National Polytechnic Institute, Mexico City, in 2001, and the Ph.D. degree from the University of Massachusetts, Amherst, MA, USA, in 2007. His Ph.D. research focused on the miniaturization, development, calibration, and performance assessment of low-cost and power-efficient microwave radiometers for remote sensing applications. From 2001 to 2005, he was a Research Assistant with the Microwave Remote Sensing Laboratory, University of Massachusetts, where he was involved in the design, development, and characterization of highly integrated multichip modules and microwave circuits for low-noise, low-power consumption, high-gain, and high-stability microwave radiometers. From 2005 to 2007, he was with the Microwave Systems Laboratory, Colorado State University, Fort Collins, CO, USA, focusing on the demonstration of a low-cost and power-efficient compact microwave radiometer for humidity profiling. From 2008 to 2018, he supported the development of operational physical retrieval systems that employ hyperspectral-infrared and microwave observations implemented for the Polar Operational Environmental Satellites Project (POES) and the Joint Polar Satellite System (JPSS). He has been a Physical Scientist with NOAA/NESDIS/Center for Satellite Applications and Research, College Park, MD, USA, since 2018, where he has led the calibration and validation of the JPSS Cross-track Infrared Sounder instruments and supports the planning of the next generation of NOAA infrared and microwave sounders. His research interests include satellite remote sensing, satellite data assimilation, inverse theory applied to geoscience fields, weather forecasting, earth system science, small satellites, and the design of radiometer systems for earth observations based on emerging technologies.

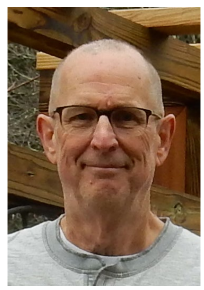

Larrabee Strow has lead the Atmospheric Spectroscopy Laboratory (ASL) group in the Physics Department at the University of Maryland Baltimore County (UMBC) since 1984. His work centers on the development and use of high-spectral resolution infrared satellite sounders. These sensors provide critical observational information to numerical weather prediction centers for preparing forecasts, while also providing new space-borne global measurements of various minor constituents (carbon monoxide, methane, dust, volcanic ash and sulphur dioxide, carbon dioxide). ASL participated in the development of three existing hyperspectral sounders (AIRS, IASI, and CrIS), especially regarding the pre- and post-launch calibration of the two U.S. instruments (AIRS, CrIS). The ASL group provides operational radiative transfer algorithms for retrievals of atmospheric profiles for the NASA EOS-AQUA AIRS instrument and for the NOAA NUCAPS retrieval system using the CrIS and IASI sounders.

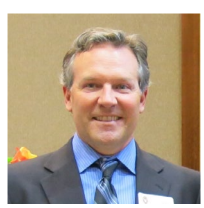

David Tobin received the B.S., M.S., and Ph.D. degrees in Physics from the University of Maryland Baltimore County, Baltimore, MD, USA in 1991, 1993, and 1996, respectively. He is a Distinguished Scientist at the Cooperative Institute for Meteorological Satellite Studies (CIMSS) within the Space Science and Engineering Center (SSEC) at the University of Wisconsin-Madison, Madison, WI, USA. His research interests include infrared molecular spectroscopy, infrared radiative transfer, hyperspectral sensor design, calibration, and data processing, and satellite inter-calibration. Dr. Tobin is a member of the International Radiation Commission, the Global Space-based Inter-

Calibration System (GSICS) Research Working Group, and the International TOVS Advanced Sounder Working Group.

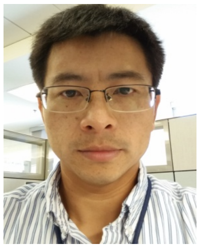

Yong Chen received the B.S. and M.S. degree in atmospheric sciences from Peking University, Beijing, China, in 1996 and 1999, respectively, and the Ph.D. degree in atmospheric sciences from University of California, Los Angeles, in 2005. Currently, he is a Physical Scientist with NOAA/NESDIS/Center for Satellite Applications and Research, College Park, MD, USA. His research interests include 1) Radiative transfer theory and applications; 2) Development and implementation of fast radiative transfer model for satellite data assimilation; 3) Radiometric and spectral calibration and validation of satellite hyper-spectral infrared sounders, IR data process; and 4) Global Navigation Satellite System Radio Occultation data processing and data assimilation.

Denis Tremblay, Physical scientist for Global Science Technology and affiliate to NOAA. Dr. Tremblay received a B.S. in Geology from Laval University in Canada, a M. Sciences and Ph. D in Aerospace engineering from the University of Colorado-Boulder. Specialties includes remote sensing, astrodynamics, and spectrometry. He contributed to the mission projects of the Tropospheric Emission Spectrometer, the MISR instrument, the S-NPP and NOAA-20 CrIS instruments with focus on calibration and validation.

Robert O. Knuteson received the Ph.D. degree in physics from the University of Wisconsin–Madison (UW-Madison), Madison, WI, USA, in 1987. Since 1987, he has been with the Space Science and Engineering Center, UW-Madison. His research interests include infrared satellite sensor calibration and atmospheric remote sensing.

David G. Johnson received the B.A. degree in physics from Pomona College in Claremont, California, in 1981 and the M. A. and Ph.D. degrees in physics from Princeton University in Princeton, New Jersey in 1984 and 1986, respectively.

From 1987 to 2000 he was a Physicist with the Smithsonian Astrophysical Observatory. Since 2000 he has been an Instrument Scientist with the Engineering Directorate, NASA Langley Research Center, Hampton, Virginia. He has served as the Joint Polar Satellite System Cross Track Infrared Sounder Instrument Scientist since 2010.

Dr. Johnson was a recipient of the NASA Silver Snoopy award in 2010, and the NASA Exceptional Engineering Achievement, Exceptional Achievement, and Distinguished Service Medals in 2011, 2014, and 2020, respectively.

Clayton Buttles

Lawrence Suwinski

Bruce P. Thomas

Adhemar R. Rivera received the B.S. degree in Aerospace Engineering and minors in Math and Naval Engineering from Virginia Polytechnic Institute and State University (Virginia Tech), Virginia, US, in 2014. While being an undergrad, Adhemar served as team lead for Virginia Tech's Atrobotics team participating in NASA's Mars Robotic Mining Competition in 2014 leading the team to the finals held at NASA's Kennedy Space Center in Florida, US. He joined the JPSS mission in 2015.

From 2015 to 2018 he helped the mission as 1553 Bus engineer with NASA's Mission Operation Support Team (MOST). His work included development of instrument procedures used for environmental testing and ground satellite integration prior to launch. In addition, he supported JPSS-1 commissioning as payload engineering monitoring and ensuring his subsystems satisfied designed expectations prior JPSS-1 was handed over to NOAA for nominal weather operations.

From 2018 to present he joined NOAA's Mission Operation Team (MOT) as the JPSS Payload Lead Engineer overseeing S-NPP and NOAA-20. He is responsible of assuring that all the instruments in both missions operate and generate science data as expected 24/7 and bringing them online in the event of any anomaly. Among other CrIS instrument related events that Mr. Rivera supported is the previous Side 2 Swap performed in June, 2019. Like the Side 1 Swap, Adhemar was responsible of planning, developing, and testing the commanding sequence in relation to the available contact times. Eventually, he successfully commanded the instrument to the desired side for nominal operations while never compromising the instrument's health and safety.

Erin Lynch received B.S. degrees in physics and mathematics in 2006 and 2010 respectively and the M.S. and the Ph.D. in Atmospheric and Oceanic Science in 2017 and 2019 respectively, all from the University of Maryland in College Park, MD, USA.

From 2019 to 2020, she was Post-Doctoral Research Associate with the Cooperative Institute for Satellite Earth System Studies (CISESS)/Earth System Science Interdisciplinary Center (ESSIC), University of Maryland, College Park, MD, USA. Since 2020 she has been a Remote Sensing Scientist with Global Science and Technology, Inc. She supports the CrIS SDR Team at NOAA/NESDIS/STAR providing post-launch monitoring and assessment of the geometric calibration of the CrIS sensors and inter-calibration with other hyperspectral infrared sounders.

Kun Zhang (M'16) received the B.S. degree in electrical engineering from the Beijing University of Aeronautics and Astronautics, Beijing, China, in 1997, the M.S. degree in electrical and computer engineering from the University of Florida, Gainesville, FL, USA, in 2000, and the Ph.D. degree in electrical engineering from the University of Colorado at Boulder, Boulder, CO, USA, in 2018.

In 2000, he joined Vexcel Corporation, Boulder, as a Software Engineer and worked on the development of synthetic aperture radar (SAR) data processing and image formation algorithms. From 2007 to 2012, he became a Senior Software Development Engineer with Microsoft Corporation, Redmond, WA, USA, where he completed an SAR image processing system specifically for supporting the NASA MiniRF Lunar Mission. In 2013, he joined Center for Environmental Technology (CET), University of Colorado at Boulder, as a Research Assistant for radiative transfer modeling and satellite microwave radiances assimilation. Since 2019, he joined Global Science and Technology, Inc. (GST), Greenbelt, MD, USA as a remote sensing scientist and is currently working for the NOAA/STAR CrIS SDR calibration and validation science team. His research interests include hyperspectral infrared sensor calibration and validation, radiative transfer theory, microwave and infrared radiances assimilation, non-spherical hydrometeor scattering modeling, and satellite system design for high spatio-temporal resolution observations.

Zhipeng (Ben) Wang received the B.S. and M.S. degrees in Optoelectronics from Department of Precision Instrument and Mechanology from Tsinghua University, Beijing China in 2000 and 2003 respectively, and the Ph.D. degree in optics from the University of Arizona, Tucson, Arizona USA in 2008.

He is currently an associate research scientist of University of Maryland's Earth System Science Interdisciplinary Center, supporting the calibration and validation of JPSS CrIS instrument.

Warren D. Porter was born in Concord, Massachusetts. He received a B.S. degree from SUNY Stony Brook in 2013, double majoring in both atmospheric & oceanic Sciences as well as applied mathematics & Statistics. He also minored in chemistry and physics.

From 2013 to 2014 he interned for Atmospheric & Environmental Research, Inc and its parent company Verisk Analytics. From 2014 to 2017, he was a doctoral student at the University of Maryland in College Park studying Atmospheric & Oceanic Science. In 2018, he joined Science Systems and Applications, Inc as a scientific analyst assisting the Integrated Calibration Validation System and Long Term Monitoring (ICVS-LTM) group at NOAA NESDIS STAR. His research interests include data visualization, machine learning and data science.

In 2019, Mr. Porter presented a poster at the Joint Satellite Conference hosted in Boston, MA by EUMETSAT, NOAA and the American Meteorological Society (AMS) as well as at the first annual NOAA Workshop on Leveraging AI in Environmental Science. In 2020, he coauthored his first peer reviewed research article.

Xin Jin received the B.S. and M.S. degrees from the Nanjing Institute of Meteorology, Nanjing, China, in 1997 and 2000, respectively, and the Ph.D. degree in atmospheric physics from Peking University, Beijing, China, in 2003. From 2003 to 2006, he was with the University of Manitoba, Winnipeg, MB, Canada, conducting research on arctic cloud and radiative flux processes. He was with the Cooperative Institute for Meteorological Satellite Studies, Space Science and Engineering Center, University of Wisconsin, Madison, from 2006 to 2011, conducting research in the retrieval of trace gas and the atmospheric profile sounding techniques from geostationary satellites. He has been working on CrIS calibration at NOAA/NEDSIS/STAR since 2011.

Joseph P. Predina (M'73-L'19) was born in Cleveland, Ohio, USA in 1953. He received the B.S. degree in electrical engineering from Purdue University, West Lafayette, Indiana, in 1975 and the M.S. degree in electrical engineering from Purdue University, West Lafayette, Indiana, in 1976.

From 1976 to 1981, he was a communication system research engineer for Motorola in Schaumburg, Illinois. Between 1981 and 2013 he was systems engineer and then Tech Fellow at ITT/Exelis/Harris in Fort Wayne, Indiana where he developed visible and infrared remote sensors for NOAA and NASA weather satellite systems such as GOES I-M and CrIS. In 2013, he became President and founder of Logistikos Engineering LLC, a small aerospace firm in Fort Wayne, Indiana that specializes in space borne remote sensor technology research and development.

Reima I. Eresmaa was born in Jyväskylä, Finland in 1977. He received the M.Sc. and Ph.D. degrees in meteorology from the University of Helsinki, Finland, in 2001 and 2007, respectively.

From 2001 to 2009, he worked as a Scientist at the Finnish Meteorological Institute in Helsinki, Finland, and focused on meteorological application of ground-based measurement data from Global Navigation Satellite Systems. From 2009 to 2020, he was a Scientist at the European Centre for Medium-range Weather Forecasts, where he contributed to the development of data assimilation methods and the use of satellite data in numerical weather prediction. He returned to the Finnish Meteorological Institute as a Scientist in 2020, and has held the position of Group Leader since May 2021. His current research interests include regional and limited-area applications of numerical weather prediction.

Dr. Eresmaa was a recipient of the Young Scientist Travel Award of European Meteorological Society in 2007. He has been a member in the IASI and IASI-NG Sounder Science Working Group since 2017.

Andrew Collard

Benjamin Rushton is a Meteorologist in the Data Assimilation Section at the Naval Research Laboratory Marine Meteorology Division in Monterey, CA. He completed a M.S. (2000) and Ph.D. (2004) in Atmospheric Sciences from Colorado State University (CSU).

From 2004 to 2006, he served as a National Academy of Sciences Post-Doctoral Fellow at NRL, and from 2006 to the present has worked in federal service for NRL. He has worked closely with other agencies in the U.S. such as NOAA and NASA and with the Joint Center for Satellite Data Assimilation (JCSDA). He is active in the International TOVS and Radio Occultation Working Groups (ITWG and IROWG) or the Coordination Group for Meteorological Satellites (CGMS) and is a co-chair of the International Earth Surface Working Group. His specialties include satellite meteorology, remote sensing from infrared and microwave sensors, GNSS radio occultation and data assimilation theory for numerical weather prediction.

James A. Jung was born in Benton Harbor, MI in 1963. He received a B.S. Degree in Atmospheric Sciences from Purdue University in 1985, an Airman's Certificate (Private Pilot) in 1987, a M.S degree in Atmospheric Sciences from South Dakota School of Mines and Technology in 1989, and a Ph.D in Atmospheric and Oceanic Sciences from the University of Maryland in 2008.

From 1987 – 1990 he was a forecaster and chief meteorologist for the North Dakota Atmospheric Resource Board overseeing weather modification activities for North Dakota. From 1990 – 1998 he was a forecaster, research and mission meteorologist for Aeromet, Inc. providing mission specific weather support for the U.S. Army at Kwajalein Atoll. Since 1998 he has been a research scientist at the University of Wisconsin conducting data assimilation experiments with NOAA/NWS, specializing in the use of satellite weather observations.

Christopher D. Barnet received a B.S. degree in electronics technology (1976) and M.S. degree in solid state physics (1978) from Northern Illinois University, DeKalb. In 1990 he received his Ph.D. degree from New Mexico State University, Las Cruces in the remote sensing of planetary atmospheres. His postdoctoral research focused on ultraviolet, visible, and near-infrared observations of the outer planets using a wide variety of instruments on-board the Voyager spacecraft and the Hubble Space Telescope. Since 1995 he has worked on advanced algorithms for terrestrial hyper-spectral infrared and microwave remote sounding supporting both NASA and NOAA missions. In 2013 he joined Science and Technology Corporation to support new applications for these advanced algorithms and now serves as a NOAA Joint Polar Satellite System (JPSS) Program Science subject matter expert for hyperspectral IR soundings. From 2014 to 2021 he was selected to lead the sounding discipline team of the NASA Terra-Aqua-Suomi National Polar-orbiting Partnership (TASNPP) science team and has worked development long-term datasets from sounding instruments aboard the Aqua, Suomi-NPP and JPSS satellites**.**

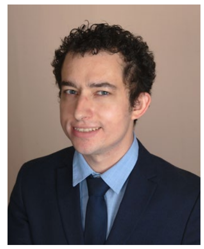

Peter J. Beierle received the B.S. degree in physics and mathematics from Stony Brook University in New York in 2011 and a Ph.D. in Physics from the University of Nebraska-Lincoln in Nebraska in 2017. There, his Ph.D. research focused on experimental tests of the foundations of quantum mechanics using matter-wave optics.

In 2019, Peter joined the Cooperative Institute for Satellite Earth System Studies at the University Maryland to work with the CrIS SDR Team at NOAA/STAR. There, he works on various Cal/Val activities including CrIS instrument monitoring, calibration and validation of the instruments, and preparations for JPSS-2 and JPSS-3 CrIS.

Banghua Yan received the Ph.D. degree in atmospheric physics from the Institute of Atmospheric Physics, Chinese Academy of Sciences, Beijing, China, in 1997 and the Ph.D. degree in atmospheric radiation from the University of Alaska, Fairbanks, in 2001. She is currently a physical scientist with the Satellite Calibration and Data Assimilation Branch in the NOAA Center for Satellite Applications and Research (STAR). From November 1999 to July 2010, she worked for the STAR through companies or NOAA Joint Center for Satellite Data Assimilation (JCSDA) or the Earth System Science Interdisciplinary Center in University of Maryland. During this period, she significantly contributed to the developments of microwave land, snow, and sea ice emissivity models, and microwave satellite instrument data assimilation studies. Those work have significantly improved the use of satellite sounding data in numerical weather prediction (NWP) models. The land, snow, and sea ice microwave emissivity models have been implemented into the NOAA NCEP NWP model and the JCSDA community radiative transfer model that has been successfully used in several operational data assimilation systems in the U.S. From August 2010 to August 2017, she was an Oceanographer with the NOAA Office of Satellite Data Processing and Distribution, Camp Springs, MD, to lead the NOAA operational ocean color production system. She has published approximately 30 papers in international peer-reviewed journals as the first or co-author. In addition, from September 2017 to September 2019, she successfully led calibrations/validations of Metop-C Advanced Microwave Sounding Unit-A (AMSU-A) to ensure the operation of AMSU-A data. She also coordinated the JPSS/STAR (JSTAR) mission program for more than half years. Currently, she leads calibrations/validations of Joint Polar Satellite System Ozone Mapping and Profiler Suite (OMPS) and the STAR Integrated Calibration/Validation System (ICVS) Long-term Monitoring.

Daniel Mooney

Henry Revercomb